**Article:**

Colombo, M and Fairweather, M (2015) Multiphase turbulence in bubbly flows: RANS simulations. International Journal of Multiphase Flow, 77. 222 - 243. ISSN 0301-9322

https://doi.org/10.1016/j.ijmultiphaseflow.2015.09.003

# Multiphase turbulence in bubbly flows: RANS simulations

**Marco Colombo* and Michael Fairweather**
Institute of Particle Science and Engineering, School of Chemical and Process Engineering, University of Leeds, Leeds LS2 9JT, United Kingdom
E-mail addresses: M.Colombo@leeds.ac.uk (Marco Colombo); M.Fairweather@leeds.ac.uk (Michael Fairweather)
*Corresponding Author: +44 (0) 113 343 2351

## Abstract

The ability of a two-fluid Eulerian-Eulerian computational multiphase fluid dynamic model to predict bubbly air-water flows is studied. Upward and downward pipe flows are considered and a database of 19 experiments from 6 different literature sources is used to assess the accuracy of the model, with the aim of evaluating our ability to predict these kinds of flows and to contribute to ongoing efforts to develop more advanced simulation tools. The particular focus in the work described is on the prediction of multiphase turbulence due to its relevance in the modelling of bubbly flows in general, including bubble coalescence and break-up, and boiling at a wall. Overall, a satisfactory accuracy is obtained in the prediction of liquid velocities and void fraction distributions in all conditions, including upward and downward flows, and wall-peaked and core-peaked void profiles, when values of the bubble diameter are specified from experimental data. Due to its importance for the correct prediction of the turbulence level in these flows, a bubble-induced turbulence model is introduced, starting from an existing formulation. Source terms due to drag are included in the turbulence kinetic energy and the turbulence energy dissipation rate equations of the $k$-$\varepsilon$ turbulence model, and optimization of the turbulence source gives velocity fluctuation predictions in agreement with data. After comparisons with data, improvement in the predictions of other turbulence models is also demonstrated, with a Reynolds stress formulation based on the SSG (Speziale, C.G., Sarkar, S., Gatski, T.B., 1991. Modelling the pressure-strain correlation of turbulence: An invariant dynamical system approach. J. Fluid Mech. 227, 245-272) pressure-strain model and the same bubble-induced turbulence model accurately predicting the two-phase flows and the anisotropy of the turbulence field. The same database is also exploited to evaluate different drag models and the advantages of including the effect of the bubble aspect ratio. Following experimental evidence, the model of Tomiyama et al. (Tomiyama, A., Celata, G.P., Hosokawa, S., Yoshida, S., 2002. Terminal velocity of single bubbles in surface tension dominant regime. Int. J. Multiphas. Flow 28, 1497-1519) is used which assumes that the bubble shape is closer to spherical near a wall and employs a correlation to calculate the aspect ratio. An increase in the drag coefficient due to the higher aspect ratio increases the accuracy of calculated velocity profiles in the near-wall region, even if additional validation is still required due to the possible loss of accuracy in the pipe centre.

**Keywords**: Bubbly flow; RANS modelling; multiphase turbulence; bubble-induced turbulence; bubble aspect ratio.

# 1. Introduction

Multiphase flows are found in a large variety of industrial applications, such as nuclear reactors, chemical and petrochemical processes, boilers and heat exchange devices amongst many others, and in a multitude of natural phenomena as well. The presence of multiple phases and the discontinuity of properties at the interface between the phases complicates the physics of these kinds of flows and poses great challenges to our ability to predict them. Multiphase flows are normally distinguished by the state of each phase (i.e. solid, liquid or gas, continuous or dispersed), and their inherent variety makes any sort of generalization in the modelling process extremely difficult, or even impossible in many cases. Amongst this great variety of flows, of interest in the present paper are dispersed gas-liquid flows, and in particular bubbly flows. In gas-liquid flows, the phases might be distributed in a number of different patterns (e.g. bubbly flow, slug flow, annular flow, mist flow), which strongly affects the hydrodynamics and exchanges of mass, momentum and energy between the phases and with external boundaries. In view of these complications, it is not surprising research on these flows is still ongoing within many engineering disciplines, and in relation to thermal hydraulics in particular, despite them having been studied for decades.

In the last three decades, computational fluid dynamics (CFD) has been exploited widely in all branches of engineering and in most industrial sectors. In more recent years, computational multiphase fluid dynamics has started to emerge as a promising tool for the analysis and prediction of multiphase flows. In the nuclear field, for example, which is the major driver of the present research work, such techniques hold the promise to solve thermal hydraulic and safety issues which have resisted full understanding and modelling for many years (Yadigaroglu, 2014). For the latter to be achieved, however, efforts are still necessary in regards to the development of advanced, validated simulation tools with the required modelling improvements, and, perhaps even more challenging, in the application of these techniques in reactor safety studies. In this paper, the abilities of a two-fluid Eulerian-Eulerian model to reproduce air-water bubbly flows inside pipes are evaluated and further improved. In particular, attention is focused on the simulation of bubble-induced turbulence and multiphase turbulence more generally, these being major drivers and prerequisites to the further development of multiphase flow modelling in many areas, including population balance approaches and boiling at a wall. In view of this, the more accurate prediction of the multiphase turbulence field is a crucial requirement in effecting further advances in these areas.

Even recently, application of multiphase CFD to engineering and real system-scale calculations has been limited to averaged Eulerian-Eulerian formulations coupled with Reynolds-averaged Navier-Stokes (RANS) turbulent flow modelling approaches (Prosperetti and Tryggvason, 2009). At the present time, the use of more advanced techniques such as direct numerical simulation, large eddy simulation or interface tracking techniques is mostly constrained to very simple flow conditions due to the computational resources required (Ervin and Tryggvason, 1997; Bunner and Tryggvason, 2002a,b; Toutant et al., 2008; Lu and Tryggvason, 2014). Nevertheless, developments in this field are accelerating, and these techniques are on track to provide fundamental support to conventional RANS modelling, and to generate new understanding, in the near future (Tryggvason and Buongiorno, 2010). In two-fluid Eulerian-Eulerian formulations, the phases are treated as interpenetrating continua, and the conservation equations for each phase are derived from averaging procedures that allow both phases to co-exist at any point. Averaging eliminates the small scales associated with the interfaces, for which a statistical description is only available for quantities such as the volume fraction, and expresses the probability of occurrence of a phase in space and time.

As a further consequence, interfacial mass, momentum and energy exchanges, strongly related to the interfacial structure, require explicit modelling with proper closure relations (Drew, 1983; Ishii and Hibiki, 2006; Prosperetti and Tryggvasson, 2009).

Over the years, adiabatic bubbly flows have been investigated by numerous researchers, and noteworthy advances in our ability to predict them have been made. Significant improvements were achieved in the description of closure terms necessary to express the forces acting on bubbles (Lucas et al., 2007; Hosokawa and Tomiyama, 2009; Lucas and Tomiyama, 2011), the interactions between bubbles and the continuous medium, and amongst bubbles themselves. Bubble populations are an evolving medium, with average characteristics such as bubble diameter and concentration of interfacial area changing continuously due to processes such as bubble break-up and bubble coalescence (Prasser et al., 2007; Lucas et al., 2010). In this area, the combination of two-fluid CFD and population balance models has been the preferred approach (Yao and Morel, 2004; Liao et al., 2015). Since most of the modelling in these areas requires knowledge of the turbulent flow field (Liao and Lucas, 2009; 2010), however, multiphase turbulence needs to be accurately predicted first for any further progress to be made. The presence of bubbles modifies the structure of the liquid turbulence field and the production of shear-induced turbulence (Lance and Bataille, 1991; Shawkat et al., 2007), which in turns modifies bubble distribution and break-up and coalescence processes. Bubbles act as a source of bubble-induced turbulence, also causing turbulence generation in flows that would otherwise be laminar (Hosokawa and Tomiyama, 2013). The net result can be the suppression or augmentation of turbulence depending on the particular flow conditions (Wang et al., 1987; Liu and Bankoff, 1993a,b; Hosokawa and Tomiyama, 2009).

During 1970-1990, many attempts were made to model turbulence in multiphase flows. The first works were based on ad-hoc phenomenological modifications to turbulence models for the liquid phase (Drew and Lahey, 1981; Sato et al., 1981; Michiyoshi and Serizawa, 1984). In general, these models include a linear superposition of the bubble-induced and shear induced-turbulence from unmodified two-equation turbulence models for the liquid phase. Notwithstanding a certain amount of success, application of these models was quite limited due to their strong dependence on experimental data, and also because multiphase turbulence is far from being a linear superposition of bubble-induced and single-phase flow turbulence, as demonstrated experimentally (Lance and Bataille, 1991; Liu and Bankoff, 1993a,b). Therefore, later works focused on the rigorous derivation of equations of turbulence in a multiphase medium. In these models, source terms due to the presence of a secondary phase were introduced directly into the equations of the turbulence model. Elgobashi and Abou-Arab (1983) derived turbulence kinetic energy and turbulence dissipation rate equations for a dilute liquid-solid, two-phase flow, applying Reynolds-averaging to instantaneous volume-averaged equations. Besnard and Harlow (1989) extended the modelling to higher volume fractions of the dispersed phase. Again, they applied Reynolds-averaging to already averaged equations. Therefore, only large-scale turbulence (with respect to the size of the particles) was treated, and closures were proposed for correlations of velocity, volume fraction and pressure fluctuations. Kataoka and Sherizawa (1989) derived a two-equation turbulence model for a gas-liquid two-phase flow using ensemble averaging of local instantaneous equations. In their model equations, closure terms including interfacial area concentration account for the interfacial transport of turbulence energy. More specifically, a drag-type source term is introduced for bubble-induced turbulence, and the generation of turbulence is allowed mainly through the drag and relative velocity between the phases.

More recently, different forms of bubble-induced source terms have been proposed and their accuracy tested through comparison against experimental data. However, no generally accepted formulation has yet emerged. In bubbly flows, the drag-type source model, where all the energy lost by bubbles to drag is converted to turbulence kinetic energy in the wakes, has been adopted in the majority of works. Crowe (2000) developed a model for turbulence generation by drag where the source term is correlated to the ratio of the dispersed phase to the turbulence length scale, which modulates the turbulence kinetic energy of the flow. The author considered mainly gas-solid particle flows, but some bubbly flows were also included in the study. Troshko and Hassan (2001), extending a two-equation turbulence model from Kataoka and Serizawa (1989), assumed bubble-induced turbulence to be entirely due to the work of the interfacial force density per unit time. Amongst the interfacial forces, only drag was considered in the model, this being generally dominant in bubbly flows. In the turbulence dissipation rate equation, the interfacial term was assumed proportional to the bubble-induced production multiplied by the frequency of bubble-induced turbulence destruction, calculated from the bubble length scale and residence time (Lopez de Berodano et al., 1994a). Politano et al. (2003) developed a $k$-$\varepsilon$ model with a bubble-induced source term for polydispersed two-phase flows. In the turbulence dissipation rate equation, these authors adopted the single-phase turbulence timescale. Yao and Morel (2004), and previously Morel (1997), also included the contribution due to virtual mass in their turbulence source, with the timescale including the bubble diameter and turbulence dissipation rate. In Rzehak and Krepper (2013a) a comparison is proposed between different literature models, and a new model is developed by the authors that is demonstrated to be a good starting point for the improved modelling of bubble-induced turbulence. The use of a mixed timescale, obtained from the bubble length scale and the liquid phase turbulence velocity scale, is proposed.

With respect to the aforementioned contributions which made use of two-equation turbulence models, comparatively fewer efforts have been dedicated to the development of Reynolds stress models (RSM) for two-phase bubbly flow, despite their ability to overcome known shortcomings of eddy viscosity-based approaches. Lopez de Bertodano et al. (1990) developed a RSM for two-phase flow based on the single-phase model of Launder et al. (1975). Bubble-induced turbulence is accounted for by work due to the drag force, and the single-phase turbulence timescale is assumed in the turbulence dissipation rate equation. Lahey et al. (1993) and Lahey and Drew (2001) derived an algebraic RSM with linear superposition of shear-induced and bubble-induced Reynolds stresses. The bubble-induced contribution is derived from inviscid flow theory and cell model averaging (Nigmatullin, 1979). Recently, Mimouni et al. (2010; 2011) developed a RSM for application in nuclear reactor thermal hydraulics. It is stated in their work that bubble-induced turbulence is included via a correlation between pressure and velocity fluctuations at the interface between the phases, with the single-phase turbulence timescale used in the turbulence dissipation rate equation. Comparison with bubbly flow experiments in a 2 × 2 rod bundle shows the improved accuracy of the RSM with respect to a $k$-$\varepsilon$ model in these conditions. In view of the lack of attention received by Reynolds stress formulations, many areas require further investigation. Amongst these, the ability of advanced turbulence modelling approaches such as that of Speziale et al. (1991) to predict the multiphase turbulence field, and the effect of the addition of bubble-induced source terms, require further examination, with more comprehensive validation against available data also necessary.

The prediction of multiphase turbulence and the simulation of gas-liquid bubbly flows are the principal subjects of this paper. More specifically, further development of a bubble-induced turbulence model and a Reynolds stress-based multiphase formulation, and their validation over a wide range of bubbly flows, are the main objectives. To facilitate the validation, air-water bubbly flows in vertical pipes have been chosen as test cases since they provide relatively simple flow conditions and have also been tested in numerous experimental works. In view of the lesser attention they have received in the literature (Lopez de Bertodano et al., 1990; Troshko and Hassan, 2001), the database is extended to include some downward flow conditions. Once assembled, the experimental database is also exploited to compare the accuracy of different drag models. Numerous drag correlations have been proposed for bubbly flows (Ishii and Zuber, 1979; Wang, 1994; Tomiyama et al., 1998), but the effect of bubble aspect ratio on drag has only recently started to be taken into account in CFD models. Amongst others, the correlation of Tomiyama et al. (2002a) was found to give the best agreement against an extended database of bubble terminal velocities in stagnant liquid (Celata et al., 2007). Hosokawa and Tomiyama (2009), combining the Tomiyama et al. (2002a) correlation with a correlation for the bubble aspect ratio, showed that the increase in bubble aspect ratio near a solid wall increases drag and reduces the relative velocity between the phases, improving agreement with experiments in that region. To further improve phase velocity predictions, in this work the correlation of Tomiyama et al. (2002a) is compared with other drag models and validated against the extended database.

It was mentioned above how convincing validation against multiple experimental data sets is a fundamental step towards the confident utilization of any multiphase CFD methodology. This paper takes advantage of the large amount of experiments made with air-water pipe flows. Serizawa et al. (1975a-c) studied experimentally air-water upward flows in a 60 mm ID pipe at atmospheric pressure. Both wall- and core-peaking void profiles were observed as a function of the bubble diameter. At high liquid velocity, liquid-phase velocity fluctuations were reduced with an increase in the gas flow rate at low gas flow rates, but increased again with further increases of the latter flow rate. Wang et al. (1987) investigated bubbly air-water upward and downward flows in pipes. Liquid velocity, void fraction and Reynolds stresses were measured. Generally, wall-peaked void profiles were associated with upward flows and core-peaked void profiles with downward flows. Turbulence was increased by the presence of bubbles in the majority of cases, and turbulence suppression was only observed at high liquid flow rates and low void fraction. Lance and Bataille (1991) studied a grid-generated turbulent bubbly flow in a square channel at atmospheric pressure. Based on their results, the amount of bubble-generated turbulence is strongly dependent on the void fraction. At very low void fraction, the turbulence can be considered as the simple superposition of shear- and bubble-induced components. However, over a certain value ($\alpha > 1$ %), the relation becomes highly non-linear and the bubble-induced component dominates. Liu and Bankoff (1993a,b) performed experiments for air-water bubbly upward flows in a 38 mm ID pipe. These authors created an extensive database covering a large range of flow conditions for wall- and core-peaked void profiles, with turbulence augmentation and suppression observed. Nakoryakov et al. (1996) measured the flow and turbulence characteristic of a downward air-water flow in a 42.3 ID pipe and of an upward air-water flow in a 14.8 mm ID pipe. Core-peaked void profiles were observed in downward flows. Generally, the presence of the bubbles increased the turbulence in the core region, whereas lower wall shear stress and velocity fluctuations were measured near the wall, with respect to a single-phase flow. Liu (1997, 1998) studied upward air-water bubbly flows at different bubble diameters and for the same water and air fluxes. Measurements provide an indication on the effect of bubble size on phase velocities, turbulence fluctuations, turbulence suppression and augmentation, and the wall shear stress, for both wall- and core-peaked void profiles. Kashinsky and Radin (1999) studied the turbulence structure of an air-water downward bubbly flow inside a 42.3 mm diameter pipe. Liquid velocity, void fraction, velocity fluctuations and wall shear stress were measured with changes in the bubble diameter at constant water and air flow rates. These authors reported an increase of the wall shear stress with respect to a single-phase flow. At the same time, a decrease in the wall shear stress fluctuations and turbulence suppression near the wall were observed. In general, the single-phase law-of-the-wall also remained valid in bubbly downward flow. Hibiki and Ishii (1999) and Hibiki et al. (2001) measured void fraction, interfacial area concentration, bubble diameter, phase velocities and liquid velocity fluctuations profiles for upwards air-water flows in 25.4 mm and 50.8 mm ID pipes. Although measurements were mainly intended to support development of constitutive relations for the interfacial area concentration equation, velocity fluctuation measurements are provided for a significant range of bubbly flows covering finely dispersed bubbly flows, and bubbly to slug flow transition as well. So et al. (2002) measured the turbulence structure of a monodispersed 1 mm bubble diameter bubbly upward flow inside a rectangular duct using laser Doppler velocimetry. At void fractions close to 1 %, wall-peaked void profiles were observed, characterized by flatter velocity profiles, as well as augmentation of near-wall turbulence and suppression of velocity fluctuations in the duct centre. Shawkat et al. (2007; 2008) investigated the bubble and liquid turbulence characteristics of an air-water bubbly flow inside a large 200 mm diameter pipe. Measurements for wall- and core-peak void profiles highlighted a general increase of the turbulence when bubbles were introduced, except for high liquid velocity and low void fraction conditions, where turbulence suppression was more often observed. The presence of bubbles changed the turbulence energy spectrum, causing a shift of the energy to lower length scales that are of the order of the bubble diameter. Hosokawa and Tomiyama (2009) presented measurements of the radial distribution of void fraction, bubble aspect ratio, phase velocities, turbulence kinetic energy and Reynolds stresses for an upward air-water bubbly flow in a 25 mm ID pipe. Turbulence suppression was observed at high liquid velocity, whereas turbulence augmentation was more typical of low liquid velocity conditions. The aspect ratio of bubbles was also increased by the presence of the wall, which induced an increase of the drag coefficient and a decrease of the relative velocity between the phases in the near-wall region.

At the beginning of this work, starting from the bubble-induced turbulence model of Rzehak and Krepper (2013a), validation is extended to a wider range of experiments and a further optimization of the model is proposed, which is then compared against the Rzehak and Krepper (2013a) model itself and the model of Troshko and Hassan (2001). The same bubble-induced turbulence model is then added to a multiphase Reynolds stress formulation. The latter approach is then validated against the same experimental database and the way in which wall effects are incorporated in the pressure-strain correlation, and their coupling with the two-phase flow field, are discussed. Later, the database is exploited to compare different drag models, and their behaviour in the near-wall region in particular, and finally the validation of the CFD model is extended to downward pipe flows. In Section 2, the experimental database is presented in more detail. Section 3 describes the CFD model, and simulation results are discussed from Section 4. Finally, conclusions and some further developments are provided in Section 5.

## 2. Experimental data

For confident application of multiphase CFD techniques in engineering calculations, an extensive validation is required in advance. In this work, 19 measurement sets from 6 different sources were selected, which allows validation of the models proposed over a wide range of parameters and operating conditions. The database includes measurements from

Serizawa et al. (1975a-c), Wang et al. (1987), Liu and Bankoff (1993ab), Liu (1998), Kashinsky and Radin (1999) and Hosokawa and Tomiyama (2009). These data extend to air-water upward and downward flows in pipes, characterized by both wall-peaked and core-peaked void profiles. In the majority of previous studies, validation was mainly achieved against wall-peaked profiles (Troshko and Hassan, 2001; Rzehak and Krepper, 2013a). Therefore, the present validation can be seen as a further extension of previous works in this regard alone. Details of the database are provided in Table 1. Significant ranges of void fraction $\alpha$ (0.03 – 0.45), water superficial velocity $j_w$ (0.5 – 1.4), air superficial velocity $j_a$ (0.02 – 0.436) and hydraulic diameter $D_h$ (0.025 m – 0.06 m) are covered by the database. Bubble diameters covered are mostly between 3 mm and 4.25 mm. Flows with significantly smaller bubbles are included for downward flow conditions only (0.8 mm and 1.5 mm). In addition, comparison is also provided against grid-generated turbulence data obtained for bubbly flows by Lance and Bataille (1991). Since these data were only used for validating predictions of the axial development of the turbulence, they are not included in Table 1.

Averaged values of the void fraction were not reported by all authors. For these cases, averaged values in Table 1 were derived from radial void profiles by averaging. Averaged profiles were also used to check superficial velocities and void fractions provided by the authors. In view of some discrepancies between calculated and stated values, adjustment of inlet velocity and void fraction was necessary for the cases of Serizawa et al. (1975a-c) and Wang et al. (1987). Also bubble diameter, which is a very important parameter used to characterize the modification to the continuous phase turbulence field induced by bubbles, was not available for all the experiments. For Wang et al. (1987), values were taken from Troshko and Hassan (2001). For Serizawa et al. (1975b), a value $d_B$ = 4 mm is provided by the authors but only as an average over all experiments. In Liu and Bankoff (1993a), a range between 2 mm and 4 mm is stated. Since a limited amount of information was available, a mean value over the range stated, $d_B$ = 3 mm, was chosen. In view of the observations above, it is important to stress the necessity of detailed experimental studies for proper model validation. More specifically, notwithstanding the large amount of experiments available, the majority do not provide a complete characterization of the flow. As will be shown in the following, to improve our ability to predict these kinds of flows it is desirable to have measurements of all the parameters of interest (including bubble diameter and turbulence), since they interact with each other in a complex and non-linear way.

Concerning turbulence measurements, r.m.s. of streamwise velocity fluctuations values only are provided in the majority of the papers. However, from the experiments available it is possible to see how an anisotropic turbulence field characterizes these bubbly flows. As shown in Figure 1 for cases H1, LB1 and W3 (see Table 1), considering equal radial and azimuthal normal stresses, an approximation can be obtained for the ratio of the streamwise to wall-normal r.m.s. of velocity fluctuations $u_w/v_w$ and therefore for the turbulence kinetic energy $k$. In Figure 1 as well as in the whole paper, radial profiles are presented as a function of the normalized radial coordinate $r/R$.

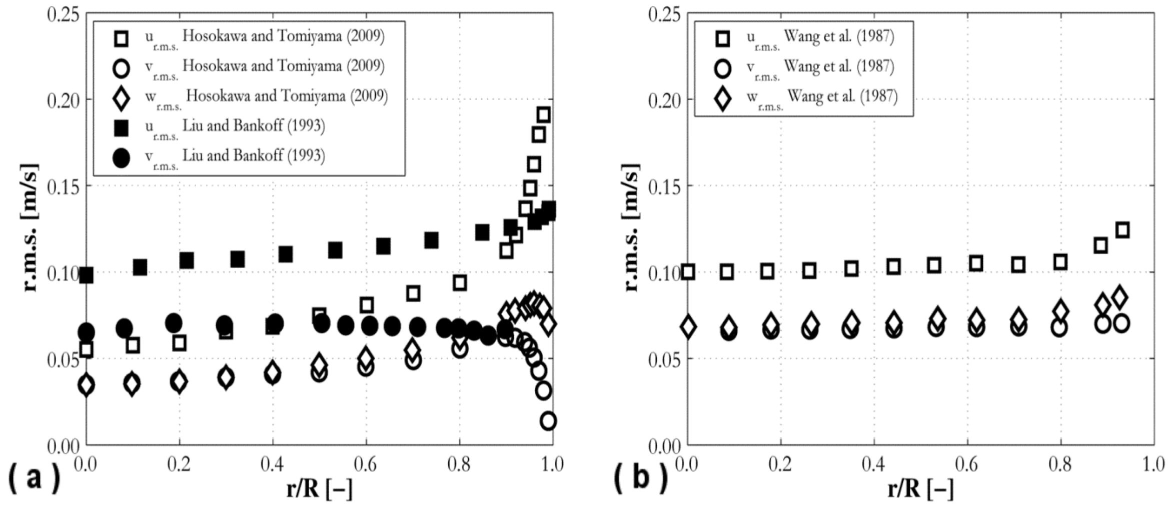


Figure 1. Experimental radial profiles for r.m.s. of velocity fluctuations: ( a ) Hosokawa and Tomiyama (2009), $j_w$ = 1.0 m/s and $j_a$ = 0.036 m/s (H1); Liu and Bankoff (1993), $j_w$ = 0.753 m/s and $j_a$ = 0.180 m/s (LB1); (b) Wang et al. (1987), $j_w$ = 0.43 m/s and $j_a$ = 0.40 m/s (W3).

In more detail, at the centre of the pipe at least ($r/R \sim 0$), a good approximation can be obtained from $v_w^2/u_w^2 \sim 0.5$, and therefore $k \sim u_w^2$. For this reason values of the streamwise r.m.s. of velocity fluctuations from experiments have been compared to $k^{0.5}$ from the simulations. The same choice was made in the work of Rzehak and Krepper (2013a), where it is also noted that $k^{0.5}/u_w$ is bounded between 0.71 for unidirectional turbulence and 1.22 for isotropic turbulence. In this way, the bubble-induced turbulence model can be optimized to predict the correct level of turbulence kinetic energy. Otherwise, a correct prediction of the streamwise r.m.s. would have resulted in an overpredicted turbulence kinetic energy. In addition, it allows a simpler extension to cover Reynolds stress formulations, which is amongst the objectives of the present paper.

Table 1. Summary of the experimental conditions included in the validation database.

| Data | Source | $j_w$ [m/s] | $j_a$ [m/s] | $\alpha$ [-] | $d_B$ [mm] | $D_h$ [m] | Profile | Orientation |
|---|---|---|---|---|---|---|---|---|
| W1 | Wang et al. (1987) | 0.71 | 0.1 | 0.100* | $3.0^+$ | 0.05715 | Wall | Upflow |
| W2 | Wang et al. (1987) | 0.94 | 0.4 | 0.202* | $3.0^+$ | 0.05715 | Wall | Upflow |
| W3 | Wang et al. (1987) | 0.43 | 0.4 | 0.383* | $3.0^+$ | 0.05715 | Wall | Upflow |
| W4 | Wang et al. (1987) | 0.668 | 0.082 | 0.152* | $3.0^+$ | 0.05715 | Wall | Downflow |
| LB1 | Liu and Bankoff (1993ab) | 0.753 | 0.180 | 0.143* | $3.0^+$ | 0.038 | Wall | Upflow |
| LB2 | Liu and Bankoff (1993ab) | 1.087 | 0.112 | 0.058* | $3.0^+$ | 0.038 | Wall | Upflow |
| LB3 | Liu and Bankoff (1993ab) | 0.376 | 0.347 | 0.456* | $3.0^+$ | 0.038 | Core | Upflow |
| LB4 | Liu and Bankoff (1993ab) | 1.391 | 0.347 | 0.210* | $3.0^+$ | 0.038 | Wall | Upflow |
| L1 | Liu (1998) | 0.5 | 0.12 | 0.152 | 2.94 | 0.0572 | Wall | Upflow |
| L2 | Liu (1998) | 1.0 | 0.22 | 0.157 | 3.89 | 0.0572 | Wall | Upflow |
| S1 | Serizawa et al. (1975a-c) | 1.03 | 0.145 | 0.107 | $4.0^+$ | 0.06 | Wall | Upflow |
| S2 | Serizawa et al. (1975a-c) | 1.03 | 0.291 | 0.192 | $4.0^+$ | 0.06 | Wall | Upflow |
| S3 | Serizawa et al. (1975a-c) | 1.03 | 0.436 | 0.259 | $4.0^+$ | 0.06 | Core | Upflow |
| H1 | Hosokawa and Tomiyama (2009) | 1.0 | 0.036 | 0.033 | 3.66 | 0.025 | Wall | Upflow |
| H2 | Hosokawa and Tomiyama (2009) | 0.5 | 0.025 | 0.04 | 4.25 | 0.025 | Core | Upflow |
| K1 | Kashinsky and Radin (1999) | 0.5 | 0.0194 | 0.0383 | 0.8 | 0.0423 | Core | Downflow |
| K2 | Kashinsky and Radin (1999) | 0.5 | 0.0924 | 0.162 | 0.8 | 0.0423 | Core | Downflow |
| K3 | Kashinsky and Radin (1999) | 1.0 | 0.0917 | 0.104 | 0.8 | 0.0423 | Core | Downflow |
| K4 | Kashinsky and Radin (1999) | 1.0 | 0.0917 | 0.108 | 1.5 | 0.0423 | Core | Downflow |

* Values calculated from radial profiles

$^+$ Values not given in original paper or averaged values

## 3. Mathematical modelling

The two-fluid Eulerian-Eulerian model solves a set of conservation equations for each phase. Adiabatic air-water flows are considered in this work, therefore only continuity and momentum equations are employed, with the phases treated as incompressible with constant properties:

$$\frac{\partial}{\partial t}(\alpha_k \rho_k) + \frac{\partial}{\partial x_i}(\alpha_k \rho_k U_{i,k}) = 0 \qquad (1)$$

$$\frac{\partial}{\partial t}(\alpha_k \rho_k U_{i,k}) + \frac{\partial}{\partial x_j}(\alpha_k \rho_k U_{i,k} U_{j,k}) = -\alpha_k \frac{\partial}{\partial x_i} p_k + \frac{\partial}{\partial x_j}\left[\alpha_k\left(\tau_{ij,k} + \tau_{ij,k}^{Re}\right)\right] + \alpha_k \rho_k g_i + M_{i,k} \qquad (2)$$

In the above equations, $\alpha_k$ represents the volume fraction of phase k, whereas in the following $\alpha$ will be used to specify the void fraction of air. $\rho$ is the density, $\boldsymbol{U}$ the velocity, $p$ the pressure and $\boldsymbol{g}$ the gravitational acceleration. $\boldsymbol{\tau}$ and $\boldsymbol{\tau^{Re}}$ are the laminar and turbulent stress tensors, respectively, and $M_k$ accounts for momentum exchanges between the phases due to the interfacial force density. In this work, drag force, lift force, wall force and turbulent dispersion force are included. Following previous studies (Politano et al., 2003; Yeoh and Tu, 2006; Krepper et al., 2013; Rzehak and Krepper, 2013a) the virtual mass is neglected due to its small effect, so that:

$$\boldsymbol{M}_k = \boldsymbol{F}_d + \boldsymbol{F}_l + \boldsymbol{F}_w + \boldsymbol{F}_{td} \tag{3}$$

### 3.1 Interphase forces

The drag force is an expression of the resistance opposed to bubble motion relative to the surrounding liquid. The momentum source due to drag is expressed as:

$$\boldsymbol{F}_d = \frac{3}{4}\frac{C_D}{d_B}\alpha\rho_c|\boldsymbol{U}_r|\boldsymbol{U}_r \tag{4}$$

Here, $U_r$ is the relative velocity between the phases and the subscript $c$ identifies the continuous phase, which is water for all the experiments in Table 1. Numerous correlations for the drag coefficient $C_D$ have been proposed over the years. In this work, three correlations are tested and compared. The Wang (1994) correlation was derived for air-water bubbly flows in near atmospheric pressure, using curve-fitting of measurements of single bubbles rising in water:

$$C_D = \exp\left[a + b\ln(Re_d) + c\left(\ln(Re_d)\right)^2\right] \tag{5}$$

The Reynolds number of the dispersed phase is expressed as a function of relative velocity and bubble diameter ($Re_d = \rho_c U_r d_B / \mu_c$, where $\mu_c$ is the dynamic viscosity of the continuous phase). Values of the coefficients *a, b* and *c* as a function of the Reynolds number can be found in Wang (1994) and the STAR-CCM+ code (CD-adapco, 2014). A great deal of work on the modelling of the drag coefficient has been undertaken by Tomiyama and co-workers (Tomiyama et al., 1998; 2002a). In Tomiyama et al. (1998), a correlation is derived where the drag coefficient is function the bubble Reynolds and Eotvos numbers ($Eo = \Delta\rho g d_B / \sigma$, where $\sigma$ is the surface tension). Here, the formulation for a contaminated system is considered:

$$C_D = \max\left[\frac{24}{Re_d}\left(1 + 0.15 Re_d^{0.687}\right), \frac{8Eo}{3(Eo + 4)}\right] \tag{6}$$

Later, Tomiyama et al. (2002a) proposed a more theoretical formulation, where the effect of the bubble aspect ratio is also accounted for:

$$C_D = \frac{8}{3}\frac{Eo}{E^{2/3}(1 - E^2)^{-1}Eo + 16E^{4/3}}F^{-2} \tag{7}$$

Here, *F* is also a function of the bubble aspect ratio *E.* The effect of aspect ratio on the drag coefficient has been discussed in detail by Hosokawa and Tomiyama (2009). Generally, experimental evidence shows an aspect ratio closer to 1 near a solid wall, which causes an increase in the drag coefficient in the near-wall region. Since knowledge of the aspect ratio is necessary for Eq. (7) to be used, a correlation was also provided. In this work, a slightly different formulation is used to correlate the aspect ratio to the distance from the wall $y_w$ based on that used by Hosokawa and Tomiyama (2009):

$$E = \max\left[1.0 - 0.35\frac{y_w}{d_B}, E_0\right] \quad (8)$$

$E_0$ is calculated from Welleck et al. (1966):

$$E_0 = \frac{1}{1 + 0.163Eo^{0.757}} \quad (9)$$

Accordingly to Legendre and Magnaudet (1998), the drag coefficient is increased by the presence of a velocity gradient in the liquid. This increase was quantified by the authors through a multiplier which is a function of the dimensionless shear rate $Sr$:

$$\varphi = 1 + 0.55Sr^2 \quad (10)$$

The dimensionless shear rate ($Sr = d_B\omega/U_r$) is calculated from the bubble diameter, the magnitude of the liquid velocity gradient $\omega$ and the relative velocity. In this work, a correction introduced by Tomiyama et al. (1998) to account for drag reduction due to bubble swarm is also considered:

$$C_D = C_{D,0}\alpha^{-0.5} \quad (11)$$

Each bubble moving in a shear flow experiences a lift force perpendicular to its direction of motion. This lift force contributes with a momentum source equal to (Auton, 1987):

$$\boldsymbol{F}_l = C_L \alpha \rho_c \boldsymbol{U}_r \text{ x } (\nabla \text{ x } \boldsymbol{U}_c) \quad (12)$$

In a pipe, the lift force has a strong influence on the radial movement of the bubbles and therefore makes a significant contribution to the void fraction radial distribution. Generally, a positive value of the lift coefficient characterizes spherical bubbles, which are therefore pushed towards the pipe wall by the lift force (Tomiyama et al., 2002b). Over the years, a plethora of different models and correlations have been proposed for the lift coefficient. A thorough review is provided in Hibiki and Ishii (2007). Amongst others, the correlation of Tomiyama et al. (2002b), where the lift coefficient is expressed as a function of the Eotvos number, has been adopted in numerous previous investigations (Krepper et al., 2008, Rzehak and Krepper, 2013a). Here, instead, a constant value of $C_L = 0.1$ has been chosen, following the observation of large discrepancies between calculations and experiments using the Tomiyama et al. (2002b) correlation. In the past, a constant value was adopted by more than one author and good agreement was reported with data for values ranging from 0.01 (Wang et al., 1987; Yeoh and Tu, 2006) to 0.5 in solutions for an inviscid flow around a sphere (Auton, 1987; Morel, 1997; Mimouni et al., 2010). Due to the extended range of values reported in the literature, it is difficult to make further comments on the accuracy of the different lift models. However, it is interesting to note that $C_L = 0.1$ was adopted by other researchers who reported good agreement with experimental measurements (Lopez de Bertodano et al., 1994b; Lahey and Drew, 2001). When bubbles grow over a certain diameter and are deformed by inertial forces, the lift force changes sign and starts to push bubbles towards the pipe centre (Ervin and Tryggvason, 1997; Tomiyama et al., 2002b; Lucas et al., 2005). This change of sign is generally predicted by most of the available correlations (Moraga et al., 1999; Tomiyama et al., 2002b), although the bubble size range over which this change is predicted to occur differs between correlations. In this work, the value $C_L$ = -0.05 was used in the presence of core-peaked void profiles. A similar weak lift coefficient for large bubbles is also reported in Troshko and Hassan (2001). Although a satisfactory accuracy was achieved over the whole database, the use of constant lift coefficients forces the choice between a wall- or a core-peaked void profile to be made before any simulation.

The presence of a solid wall modifies the flow field around bubbles. The liquid flow rate in the region between the bubble and the wall becomes lower than the liquid flow rate between the bubble and the outer flow. This asymmetry in the flow distribution around the bubble generates a hydrodynamic pressure difference on the bubble surface that, analogously to the wall force in lubrication theory, acts to keeps bubbles away from the wall (Antal, 1991):

$$\boldsymbol{F}_w = \max\left(0, C_{w,1} + C_{w,2}\frac{d_B}{y_w}\right)\alpha\rho_c\frac{|\boldsymbol{U_r}|^2}{d_B}\boldsymbol{n_w} \tag{13}$$

In the previous equation, $\boldsymbol{n_w}$ is the normal to the wall and $C_{w1}$ and $C_{w2}$ modulate the strength and the region of influence of the wall force. In this work, values of $C_{w1}$ = -0.055 and $C_{w2}$ = 0.09 were used after optimization with experiments. Obviously, the combination of lift and wall force drives the prediction of the radial void fraction distribution. To avoid optimization of the coefficients against single experiments and the related loss of generality of the model, once fixed the lift and wall force coefficients were maintained constant throughout the whole work. However, even if it was possible to keep the same value of the lift coefficient in all cases, modification of the velocity profile near the wall caused by the different drag models made necessary some adjustments to the wall force coefficient, which will be discussed later. In view of this, further work is necessary to ensure the availability of more general formulations of these models. Lastly, the turbulent dispersion force was modelled accordingly to Burns et al. (2004), who derived an expression by applying Favre averaging to the drag force:

$$\boldsymbol{F}_{td} = \frac{3}{4}\frac{C_D \alpha \rho_c |\boldsymbol{U}_r|}{d_B}\frac{\nu_{t,c}}{\sigma_\alpha}\left(\frac{1}{\alpha} + \frac{1}{(1-\alpha)}\right)\nabla\alpha \tag{14}$$

$\nu_{t,c}$ is the turbulent kinematic viscosity of the continuous phase and $\sigma_\alpha$ the turbulent Prandtl number for volume fraction, assumed equal to 1.0.

### 3.2 Multiphase turbulence modelling

Turbulence in the continuous phase is modelled with a multiphase formulation of the standard *k-ε* turbulence model (Jones and Launder, 1972). Turbulence field is solved for the continuous phase only, with balance equations for the turbulence kinetic energy *k* and the turbulence energy dissipation rate *ε* (CD-adapco, 2014) given as:

$$\begin{aligned}\frac{\partial}{\partial t}\left((1-\alpha)\rho_c k_c\right) + \frac{\partial}{\partial x_i}\left((1-\alpha)\rho_c U_{i,c} k_c\right) \\ = \frac{\partial}{\partial x_i}\left[(1-\alpha)\left(\mu_c + \frac{\mu_{t,c}}{\sigma_k}\right)\frac{\partial k_c}{\partial x_i}\right] + (1-\alpha)\left(P_{k,c} - \rho_c \varepsilon_c\right) + (1-\alpha) S_k^{BI}\end{aligned} \tag{15}$$

$$\begin{aligned}\frac{\partial}{\partial t}\left((1-\alpha)\rho_c \varepsilon_c\right) + \frac{\partial}{\partial x_i}\left((1-\alpha)\rho_c U_{i,c} \varepsilon_c\right) \\ = \frac{\partial}{\partial x_i}\left[(1-\alpha)\left(\mu_c + \frac{\mu_{t,c}}{\sigma_\varepsilon}\right)\frac{\partial \varepsilon_c}{\partial x_i}\right] + (1-\alpha)\frac{\varepsilon_c}{k_c}\left(C_{\varepsilon,1} P_{k,c} - C_{\varepsilon,2}\rho_c \varepsilon_c\right) \\ + (1-\alpha) S_\varepsilon^{BI}\end{aligned} \tag{16}$$

Here, $P_{k,c}$ is the production term due to shear and $S_k^{BI}$ and $S_\varepsilon^{BI}$ the source term due to bubble-induced turbulence. The turbulent viscosity $\mu_{t,c}$ is evaluated from the single-phase $k$-$\varepsilon$ formulation:

$$\mu_{t,c} = C_\mu \rho_c \frac{k_c^2}{\varepsilon_c} \tag{17}$$

Turbulence in the dispersed phase is not explicitly resolved, but it is obtained from the continuous phase predictions. This approximation, valid for dispersed two-phase flow, is justified in view of the very low value of the density ratio in air-water flows, which causes the Reynolds stress in the gas to be much smaller than in the liquid. Even if further verification is required for flows with significant void fraction (Behzadi et al., 2004), at the present time this approach is applied to the whole database, as done in the majority of the previous works (Gosman et al., 1992; Troshko and Hassan, 2001; Rzehak and Krepper, 2013a). Therefore, turbulence in the dispersed phase is directly related to the turbulence of the continuous phase through the turbulence response coefficient $C_t$:

$$k_d = C_t^2 k_c \tag{18}$$

$$\varepsilon_d = C_t^2 \varepsilon_c \tag{19}$$

For the response coefficient, the value $C_t = 1$ is chosen. Indeed, experimental measurements suggest that a value of unity is approached starting from void fractions as small as 6 % (Behzadi et al., 2004).

To account for the bubble contribution to turbulence, appropriate bubble-induced source terms are introduced in Eq. (15) and Eq. (16). In particular, the drag force is considered as the only source of turbulence generation due to bubbles (Kataoka and Serizawa, 1989; Troshko and Hassan, 2001; Rzehak and Krepper, 2013a). In more detail, all the energy lost by the bubbles to drag is assumed to be converted into turbulence kinetic energy inside the bubble wakes. In Kataoka and Serizawa (1989), generation of turbulence kinetic energy is directly related to the work of the interfacial force density per unit time. Interfacial work is assumed limited to the drag force, this being largely dominant in bubbly flows (Throsko and Hassan, 2001), even if Morel (1997) and Yao and Morel (2004) did later consider the contribution due to virtual mass. The turbulence kinetic energy source ${S_k}^{BI}$ is expressed as:

$$S_k^{BI} = K_{BI}\boldsymbol{F_d}\boldsymbol{U_r} \tag{20}$$

$K_{BI}$ is introduced for the modulation of the turbulence source. In the turbulence energy dissipation rate equation, the bubble-induced source is expressed as the corresponding turbulence kinetic energy source term multiplied by the timescale of the bubble-induced turbulence $\tau_{BI}$:

$$S_\varepsilon^{BI} = \frac{C_{\varepsilon,BI}}{\tau_{BI}} S_k^{BI} \tag{21}$$

Most previous researchers focused their work on the modelling of the timescale $\tau_{BI}$. In shear-induced single-phase flow turbulence modelling, the turbulence timescale corresponds to the lifetime of a turbulent eddy before it breaks up into smaller structures. In multiphase turbulence, the situation is more complex and the bubble-induced turbulence timescale should also be related to some velocity and length scale of the bubbles. At the present time, no generally accepted formulation has yet emerged. Some authors assumed the single-phase shear-induced turbulence timescale also for the bubble-induced source (Politano et al., 2003). Other researchers introduced different timescales, more related to the length and velocity scales of the bubbles. Troskho and Hassan (2001), using the suggestion from Lopez de Bertodano et al. (1994a), assumed the bubble induced timescale to be proportional to the bubble residence time. In this way, bubble-induced turbulence decays much faster than shear-induced turbulence (Throsko and Hassan, 2001). The turbulence energy dissipation rate source is expressed as:

$$S_{\varepsilon}^{BI} = C_{\varepsilon,BI} \frac{3C_D |\boldsymbol{U_r}|}{2C_{vm} d_B} S_k^{BI} \tag{22}$$

$C_{vm}$ is the virtual mass coefficient and $C_{\varepsilon,BI}$ = 0.44. Recently, Rzehak and Krepper (2013a) proposed a mixed timescale with the velocity scale derived from the liquid turbulence kinetic energy and the length scale set equal to the bubble diameter. This model is expected to mimic the split of eddies which move past the bubbles (Rzehak and Krepper, 2013b) and the generation of turbulence at the length scale of the bubble, which might be inferred from the shift of turbulence energy to smaller length scales observed in experiments (Lance and Bataille, 1991; Shawkat et al., 2007). After comparison with experiments, the authors suggested their model as an appropriate starting point for the further development of the bubble-induced turbulence contribution. The turbulence energy dissipation rate source term is given by:

$$S_{\varepsilon}^{BI} = C_{\varepsilon,BI} \frac{k^{0.5}}{d_B} S_k^{BI} \tag{23}$$

where $C_{\varepsilon,BI}$ = 1.0. The same turbulence dissipation rate source is employed here. In addition, the parameter $K_{BI}$ is included to modulate the turbulence kinetic energy generation. After comparison with the whole database, an optimum value $K_{BI}$ = 0.25 was chosen and this will be discussed in more detail in the results section.

In addition to the *k*-*ε* model, a multiphase Reynolds stress formulation was also used for the simulation of the liquid turbulence field. The model is based on the single-phase formulation and the transport equations for the Reynolds stresses ($R_{ij} = \tau_{i,j}^{Re}/\rho_c$) are (CD-adapco, 2014):

$$\frac{\partial}{\partial t}\left((1-\alpha)\rho_c R_{ij}\right) + \frac{\partial}{\partial x_j}\left((1-\alpha)\rho_c U_{i,c} R_{ij}\right) = \frac{\partial}{\partial x_j}\left[(1-\alpha)D_{ij}\right] + (1-\alpha)\left(P_{ij} + \Phi_{ij} - \varepsilon_{ij}\right) + (1-\alpha)S_{ij}^{BI} \tag{24}$$

$P_{ij}$ is the turbulence production. The Reynolds stress diffusion $D_{ij}$ is modelled accordingly to Daly and Harlow (1970), whilst the isotropic hypothesis is used for the turbulence dissipation rate term $\varepsilon_{ij}$. $\Phi_{ij}$ is the pressure-strain model accounting for pressure fluctuations that redistribute the turbulence kinetic energy amongst the Reynolds stress components. It is modelled accordingly to the formulation of Launder et al. (1975):

$$\Phi_{ij} = \Phi_{ij,1} + \Phi_{ij,2} \tag{25}$$

$$\Phi_{ij,1} = -C_1 \rho_c \frac{\varepsilon_c}{k_c}\left(R_{ij} - \frac{2}{3} k_c \delta_{ij}\right) \tag{26}$$

$$\Phi_{ij,2} = -C_2 \rho_c \frac{\varepsilon_c}{k_c}\left(P_{ij} - \frac{1}{3} \mathrm{tr}(P) \delta_{ij}\right) \tag{27}$$

$\delta_{ij}$ is the Kronecker delta function. Following Gibson and Launder (1978), additional wall reflection terms are needed to account for the modification of the pressure field and blockage of the transfer of energy from the streamwise to the wall-normal direction observed in the presence of a solid wall. In their original formulation, the authors proposed a linearly decreasing damping function with distance from the wall to limit its effect to the near-wall region. Colombo et al. (2015) note, however, that with a linearly decreasing function wall effects can still be significant near the axis of the flow, where they interact with the dispersed phase field introducing unphysical effects not observable in a single-phase flow. Therefore, the quadratic wall damping function proposed by Naot and Rodi (1982) was used in their work to allow a faster decay of wall effects. Wall reflection terms which are added to Eq. (25) are therefore equal to:

$$\Phi_{ij,1}^{w} = -C_1^{w} \rho_c \frac{\varepsilon_c}{k_c}\left(\overline{u_k u_m} n_k n_m \delta_{ij} - \frac{3}{2}\overline{u_k u_i} n_k n_j - \frac{3}{2}\overline{u_k u_j} n_k n_i\right)\left(\frac{k^{3/2}}{\varepsilon}\frac{1}{C_l y_w}\right)^2 \tag{28}$$

$$\Phi_{ij,2}^{w} = -C_2^{w}\left(\Phi_{km,2} n_k n_m \delta_{ij} - \frac{3}{2}\Phi_{ik,2} n_k n_j - \frac{3}{2}\Phi_{jk,2} n_k n_i\right)\left(\frac{k^{3/2}}{\varepsilon}\frac{1}{C_l y_w}\right)^2 \tag{29}$$

Later, Speziale et al. (1991) developed a more advanced model for the pressure-strain relation which is quadratically non-linear in the anisotropy tensor. This "SSG model" proved to be superior to formulations that are linear in the anisotropy tensor over a wide range of turbulent flows:

$$\Phi_{ij} = -[C_{1a}\varepsilon + C_{1b}tr(P)]a_{ij} + C_2\varepsilon\left(a_{ik}a_{kj} - \frac{1}{3}a_{mn}a_{mn}\delta_{ij}\right) + \left[C_{3a} - C_{3b}\left(a_{ij}a_{ij}\right)^{0.5}\right]kS_{ij} + C_4 k\left(a_{ik}S_{jk} + a_{jk}S_{ik} - \frac{2}{3}a_{mn}S_{mn}\delta_{ij}\right) + C_5\left(a_{ik}W_{jk} + a_{jk}W_{ik}\right) \tag{30}$$

Here, $a_{ij}$ are components of the anisotropy tensor, and $S_{ij}$ and $W_{ij}$ are the strain rate and the rotation rate:

$$a_{ij} = \frac{R_{ij} - \frac{1}{3}R_{kk}\delta_{ij}}{R_{ll}} \tag{31}$$

$$S_{ij} = \frac{1}{2}\left(\frac{\partial U_i}{\partial x_j} + \frac{\partial U_j}{\partial x_i}\right) \tag{32}$$

$$W_{ij} = \frac{1}{2}\left(\frac{\partial U_i}{\partial x_j} - \frac{\partial U_j}{\partial x_i}\right) \tag{33}$$

The bubble-induced turbulence source term is calculated using Eq. (20) and then split amongst the normal Reynolds stress components. With respect to the approach of Lopez de Bertodano et al. (1990), a higher fraction of bubble-induced turbulence source is accommodated by the streamwise direction:

$$S_{ij}^{BI} = \begin{bmatrix} 1.0 & 0.0 & 0.0 \\ 0.0 & 0.5 & 0.0 \\ 0.0 & 0.0 & 0.5 \end{bmatrix} S_k^{BI} \quad (34)$$

Values of the model coefficients used for the $k$-$\varepsilon$ model and the two Reynolds stress formulations can be found in Table 2.

Table 2. Coefficients used in the different turbulence models. GL: Gibson and Launder (1978); SSG: Speziale et al. (1991).

| | |
|---|---|
| ***k*-ε** | $\sigma_k = 1.0$; $\sigma_\varepsilon = 1.3$; $C_{1\varepsilon} = 1.44$; $C_{2\varepsilon} = 1.92$; $C_\mu = 0.09$ |
| **RSM GL** | $C_1 = 1.8$; $C_2 = 0.6$; $C_{1,w} = 0.5$; $C_{2,w} = 0.3$; $C_l = 2.5$ |
| **RSM SSG** | $C_{1a} = 1.7$; $C_{1b} = 0.9$; $C_2 = 1.05$; $C_{3a} = 0.8$; $C_{3b} = 0.65$; $C_4 = 0.625$; $C_5 = 0.2$ |

# 4. Results and discussion

In this section, simulation results are given and discussed. Numerical simulations were performed using the STARCCM+ code (CD-adapco, 2014) in a two-dimensional axisymmetric geometry. Constant inlet phase velocities and void fraction, and outlet pressure, boundary conditions were imposed. Simulations were advanced implicitly in time and, after an inlet development region, fully developed steady-state conditions were reached before recording the results. Strict convergence of residuals was ensured and the mass balance was checked to have an error always less than 0.1 % for both phases. Comparison with experiments is provided for radial profiles of liquid mean velocity (and air mean velocity when available), void fraction and streamwise r.m.s. of velocity fluctuations (or turbulence kinetic energy when available). After a mesh sensitivity study on a limited number of conditions, an equidistant structured mesh with the first grid point located close to $y^+ = 30$, which is a lower limit for the use of wall functions, was found sufficient to give mesh-independent solutions. Meshes for the remaining cases were then derived by adjusting the base case mesh to give similar resolution.

## 4.1 Single-phase results

Before addressing two-phase flows, a first set of simulations was carried out for the single-phase and comparisons against single-phase measurements from experiments H1and LB1 are provided in Figure 2. For H1, the $k$-$\varepsilon$ model, the RSM of Naot and Rodi (1982) and the SSG RSM of Speziale et al. (1991) are compared against radial profiles of velocity, turbulence kinetic energy and the r.m.s. of velocity fluctuations at $j = 1.0$ m/s (Figure 2 a-c). Generally, good agreement with the experiments is found. Similar mean velocity profiles are predicted by the three models (Figure 2a), which all underestimate the experimental data. This result is in agreement with the work of Ullrich et al. (2014), where experimental measurements were found higher with respect to the author's simulations made with a RSM, and with the DNS results of Wu et al. (2012). Major differences between the models are found for the turbulence kinetic energy, which is overestimated by the $k$-$\varepsilon$ model, and underestimated by both Reynolds stress formulations, in the pipe core region (Figure 2b). In particular, the SSG model predicts a lower turbulence kinetic energy with respect to the linear model of Naot and Rodi (1982). Discrepancies between the RSM predictions are also found for the r.m.s. of velocity fluctuations (Figure 2c). Both models underestimate the streamwise velocity fluctuation, but the SSG better reproduces the anisotropy of the turbulence. In particular, the Naot and Rodi (1982) model predicts an excessive difference between the azimuthal and the wall-normal velocity fluctuations.

Figure 2 d-f provides additional comparisons for the LB1 case. Velocity, r.m.s. of velocity fluctuations and Reynolds shear stress profiles are in agreement with experiments. Close agreement between results is found for the $k$-$\varepsilon$ and the Reynolds stress formulations, and for the two RSM predictions. Velocity fluctuations are shown in Figure 2e. Similarly to Figure 2c, the anisotropy of the turbulence field is well reproduced with a RSM, and accurate predictions of the streamwise and the wall-normal r.m.s. of velocity fluctuations are obtained. For the $k$-$\varepsilon$ model, the square root of the turbulence kinetic energy in Figure 2e also shows good agreement with the streamwise velocity fluctuations. This result supports the hypothesis discussed in Section 2, which noted that in these kinds of flow the turbulence kinetic energy, when not available from experiments, might be estimated from the streamwise velocity fluctuations ($k \sim u_w^2$).

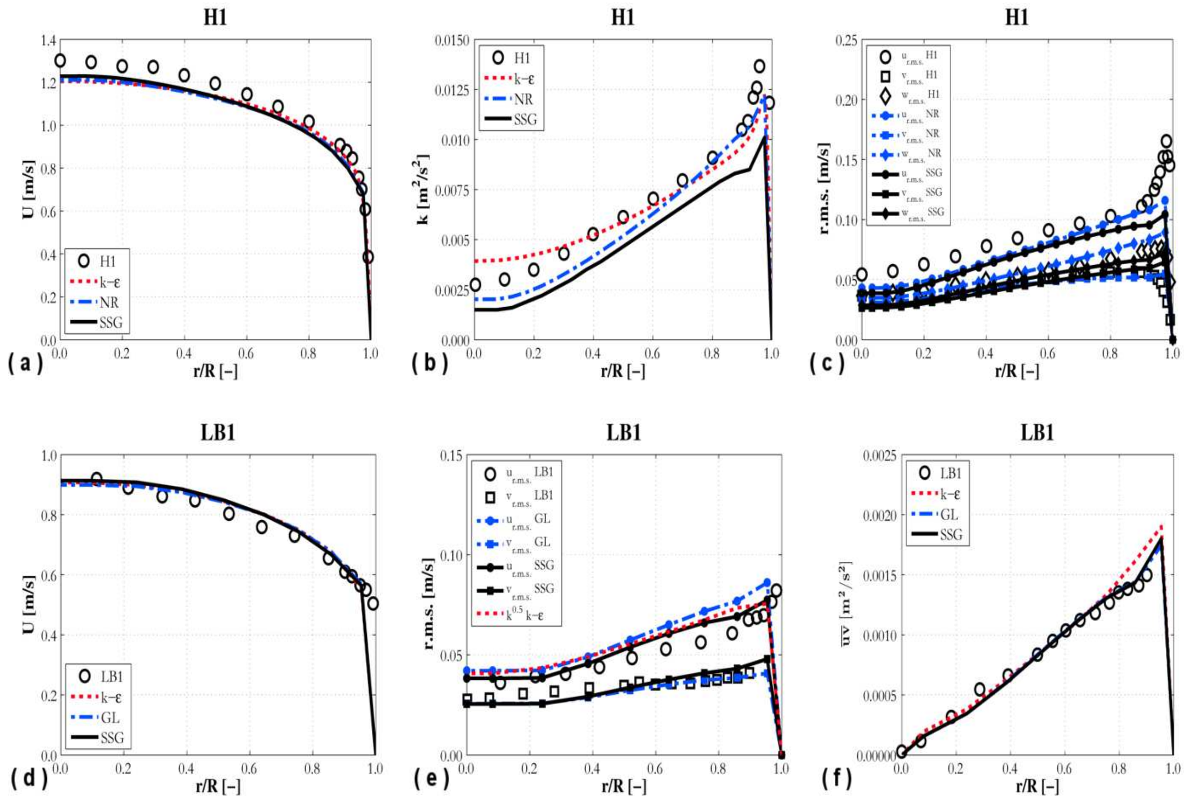


Figure 2. Radial profiles of predicted velocity, turbulence kinetic energy and velocity fluctuations from different turbulence models compared against single-phase data from experiments H1 and LB1. GL: Gibson and Launder (1978); NR: Naot and Rodi (1982); SSG: Speziale et al. (1991).

### 4.2 Bubble-induced turbulence

After the validation of the single-phase flow in the previous section, the two-phase flow is the focus from here on. In this section, the influence on liquid velocity and void fraction predictions of three different models of bubble-induced turbulence and their ability to reproduce measurements of turbulence from experiments are evaluated. Simulations are referred to as CF for the optimized bubble-induced turbulence model proposed in this work (Eq. (20) and Eq. (23)), TH for the model of Troshko and Hassan (2001) and RK for the model of Rzehak and Krepper (2013ab). Results in this section were obtained using the *k*-*ε* model and the drag model of Wang (1994). Comparisons included all the upward flow conditions with the exception of W3, which was considered only for the validation of the RSM, given in the following section. Radial profiles of water velocity, void fraction and water streamwise velocity fluctuations are shown in Figure 3, Figure 4 and Figure 5 for 9 different cases. Turbulence kinetic energy was also available for case H1 and it is shown instead of the r.m.s. of velocity fluctuations in Figure 4i.

In general, water velocity and void fraction predictions are in good agreement with experiment for all the models. Amongst the numerous experiments, core-peaked void profiles were the most difficult to predict, as shown in Figure 3 d-f for LB3 and in Figure 5 g-i for S3. For both cases, the water velocity is overestimated and the void fraction is difficult to predict because it often exhibits a mixed profile, where a significant number of spherical bubbles are still present near the wall. For such flows, it is difficult to reproduce these profiles using a constant bubble diameter. Therefore, improvements in this area are to be expected from the adoption of multi-group population balance models, which is, however, out of the scope of the present work. A better agreement is shown for wall-peaked void profiles, with the distinctive features of these flows well reproduced in the simulations. Bubbles, which maintain a shape close to spherical, are pushed towards the pipe wall by the lift force and accumulate in distinct peaks, recognisable in the void fraction radial profiles. The water flow is accelerated by the bubbles, which flow faster due to buoyancy, in particular in the near-wall region where a larger number of bubbles is present. This increase in the water velocity near the wall is responsible for the flat velocity profile that characterizes wall-peaked conditions that is also well reproduced in the simulations.

Significant differences are found between the bubble-induced turbulence models in the prediction of the r.m.s. of streamwise water velocity fluctuations. The RK model always shows the highest velocity fluctuations and, except for LB3, it overestimates the experimental measurements. In view of these results, it was decided to add the function $K_{BI}$ in Eq. (20), to limit the contribution of the bubbles to the water turbulence. Initially, some dependancy on the flow parameters, and on the bubble diameter in particular, was investigated. Since it was not possible to identify any well-defined dependancy on the flow conditions, $K_{BI}$ was set as 0.25. The uncertainity in the bubble diameter for a significant number of the experiments may have played a significant role here, preventing the identification of more complex dependancies, such as the ratio of the dispersed phase diameter to the turbulence length scale (Crowe, 2000). Therefore, limiting $K_{BI}$ to a constant value was the most appropriate choice in the present work. For further improvements, the availability of additional experimental data which include precise measurements of all the flow parameters is crucial, as already noted in Section 2. As shown from Figure 3 to Figure 5, the CF model provides satisfactory predictions for the large majority of experiments. Underestimated velocity fluctuations are only found for a limited number of data (Figure 3f) for the database of Liu and Bankoff (1993ab). This particular experiment was characterized by a relative short distance between the inlet and the measurement station. Therefore, it is possible that the conditions were not completely fully developed, causing higher velocity fluctuations with respect to the other experiments in the database. Overall, improvement with respect to the RK model is achieved.

The TH model has a global accuracy that is not dissimilar to that of the CF approach, which is even outperformed by TH in a limited number of cases. From a qualitative point of view, the radial behaviour of the streamwise r.m.s. velocity fluctuations is better reproduced by CF, except for experiment L1. In addition, TH predictions are less consistent overall and sometimes show discrepancies from the data, as is the case for experiments LB2 and S2 (Figure 3c and Figure 5f, respectively). For these experiments, the different behaviour of the turbulence also has an influence on the void fraction and liquid velocity radial profiles, which are not well predicted. Also, for experiment H1 (Figure 4 g-i), despite the more accurate prediction of the void fraction peak at the wall, a zero void fraction is predicted at the pipe centre, in contrast to both the experimental data and the other models. Finally, the increase in accuracy achieved with the CF model is more significant for core-peaked profiles (LB3 in Figure 3 d-f and S3 in Figure 5 g-i), where both RK and TH overestimate the water velocity fluctuations. Despite overpredicting the experiments, in particular near the wall, CF shows the best agreement overall. Therefore, the CF model can be considered as an improved formulation that accounts reasonably well for the bubble-induced contribution to the turbulence in bubbly flows. Obviously, further efforts are still necessary to extend the validation and to develop a more general relation for the turbulence kinetic energy source modulation ($K_{BI}$ in Eq. (20)), although the latter is subject to the availability of a larger number of detailed experimental measurements.

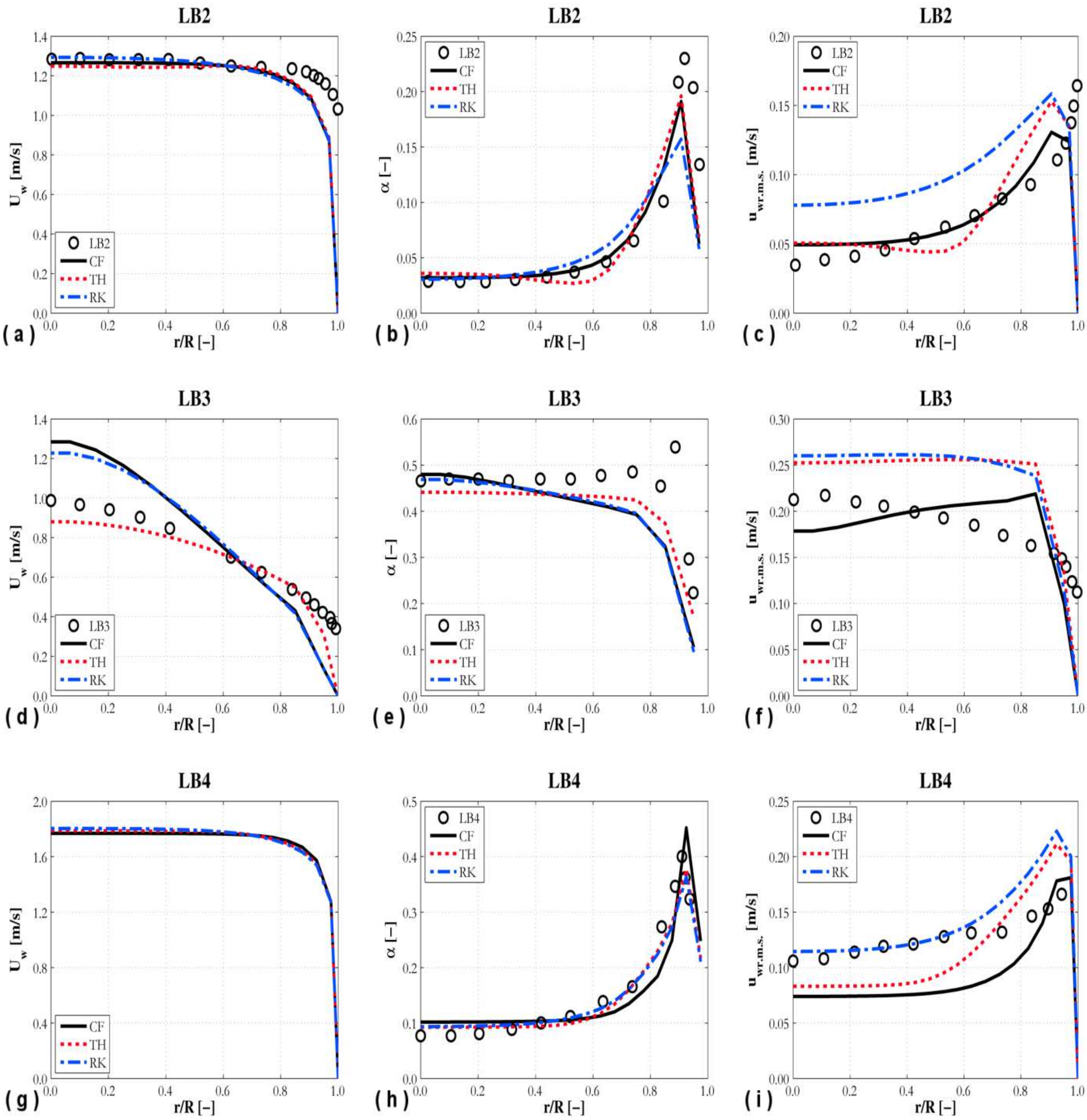


Figure 3. Radial profiles of predicted water velocity, void fraction and streamwise velocity fluctuations from different bubble-induced turbulence models compared against experiments LB2, LB3 and LB4 (from top to bottom). CF: present model (Eq. (20) + Eq. (23)); TH: Troshko and Hassan (2001); RK: Rzehak and Krepper (2013).

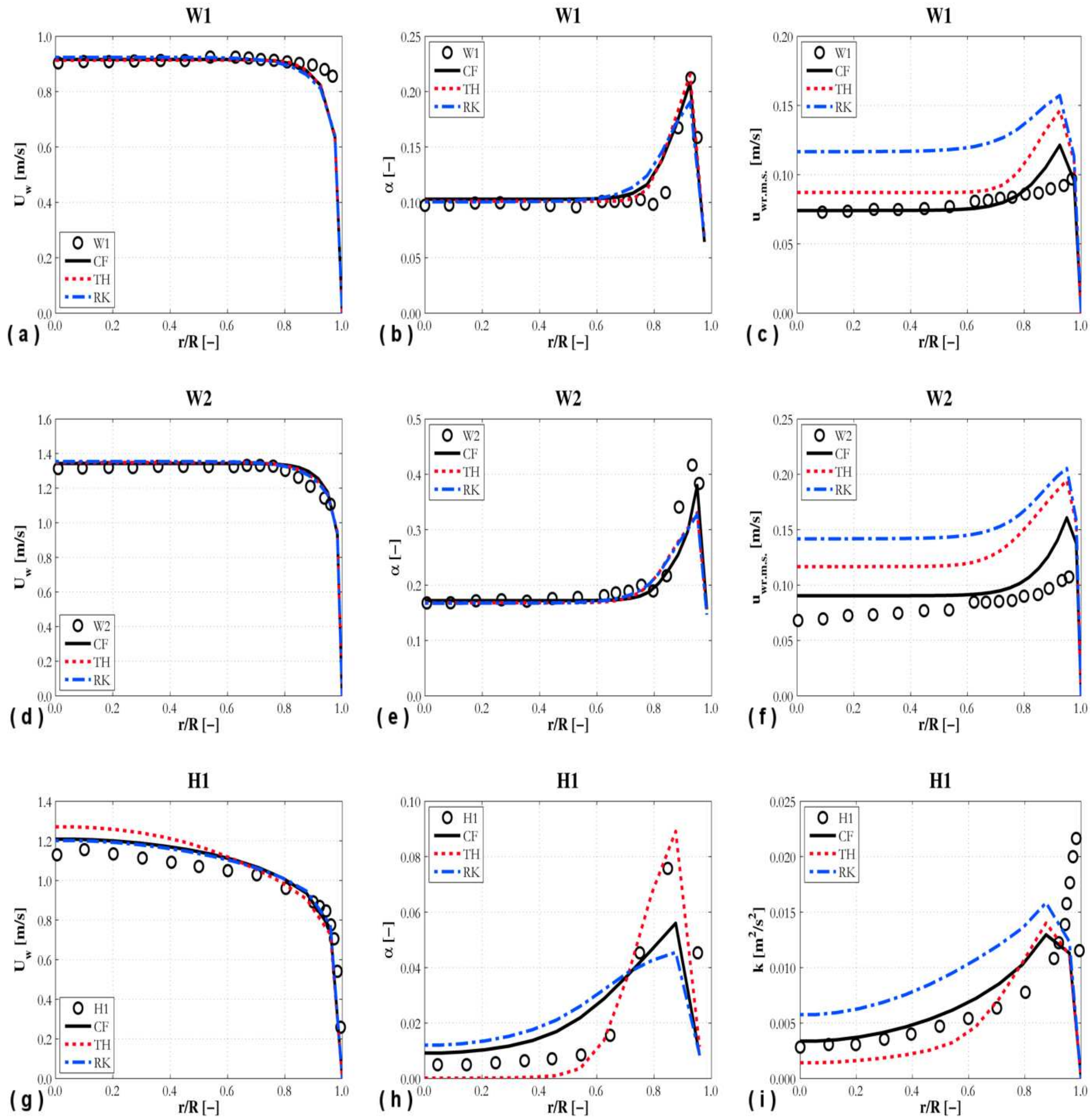


Figure 4. Radial profiles of predicted water velocity, void fraction and streamwise velocity fluctuations from different bubble-induced turbulence models compared against experiments W1, W2 and H1 (from top to bottom). CF: present model (Eq. (20) + Eq. (23)); TH: Troshko and Hassan (2001); RK: Rzehak and Krepper (2013).

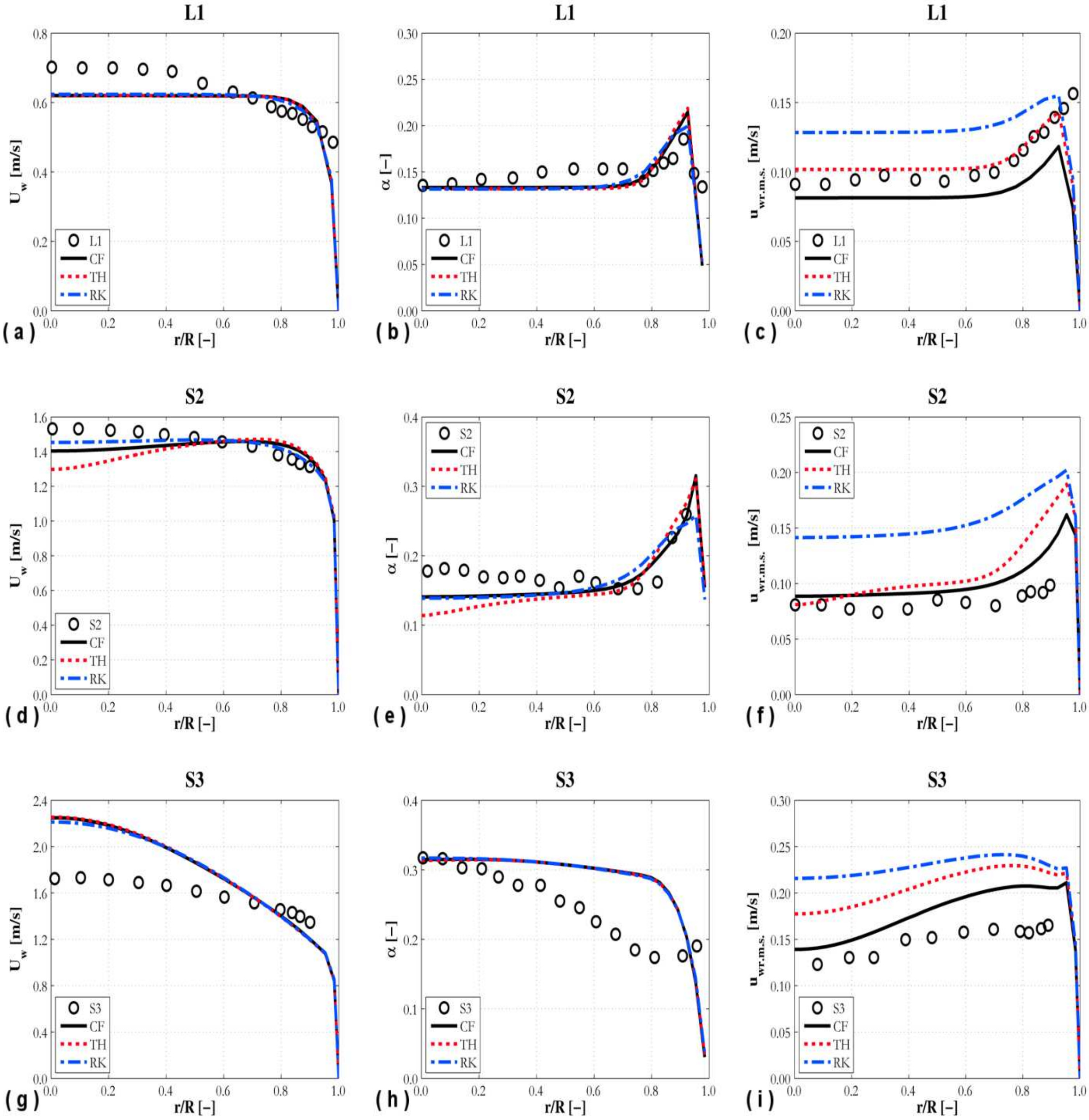


Figure 5. Radial profiles of predicted water velocity, void fraction and streamwise velocity fluctuations from different bubble-induced turbulence models compared against experiments L1, S2 and S3 (from top to bottom). CF: present model (Eq. (20) + Eq. (23)); TH: Troshko and Hassan (2001); RK: Rzehak and Krepper (2013).

### 4.2.1 Axial development of turbulence

For further validation of the bubble-induced turbulence model, comparison is also provided against measurements for a uniform, grid-generated, turbulent bubbly flow obtained by Lance and Bataille (1991). Experiments were made in a 2 m long square channel (450 mm x 450 mm), where the grid, generating the turbulence, was also equipped with injectors to blow air bubbles into the flow. Initial conditions for the simulations were taken from the turbulence measurements at the first measurement station and the evolution of the flow along the channel was followed. Comparison against the experiments is provided in Figure 6 for different values of the void fraction and for the single-phase flow. A satisfactory agreement was obtained. However, it must be pointed out that a reduction in the contribution from the bubble-induced turbulence was necessary at very low void fraction, otherwise over-prediction of the experiments would have been obtained. More specifically, a reduction of $K_{BI}$ from the optimum value (Section 3.2) of 0.25 to 0.10 was necessary at the lowest void fraction, namely 0.5 %. Then, the value was increased towards 0.25 for the higher values of the void fraction. This can be considered congruent with the findings of Lance and Bataille (1991). More specifically, they reported a linear increase of the excess turbulence kinetic energy at very low void fraction. Starting from values of the void fraction between 1 % and 2 %, strong amplification of the turbulence kinetic energy was observed, which the authors attributed to the appearance of hydrodynamic interactions between the bubbles themselves. Therefore, the experiments used to derive the value of $K_{BI}$, being all at higher void fractions, may not be representative of the region of linear increase at very low void fraction and a lower contribution from the bubbles in this region, where interactions amongst bubbles are negligible, can be expected. The amount of the bubble-induced contribution mainly affects the asymptotic equilibrium of the turbulence intensity, although the turbulence decay after the grid and the axial development of the turbulence were both well reproduced by the model. Some additional comments can be made on the value of the bubble diameter, which has a strong influence on the bubble-induced turbulence contribution. In their work, Lance and Bataille (1991) state that the experimental system was built to have 5 mm diamter bubbles and, during the experiments, bubbles were demonstrated to have a diameter of the order of 5 mm. However, detailed measurements and observations were not provided. Therefore, it is also possible that some differences in the diameter of the bubbles may have had an impact on the asymptotic bubble-induced turbulence contribution.

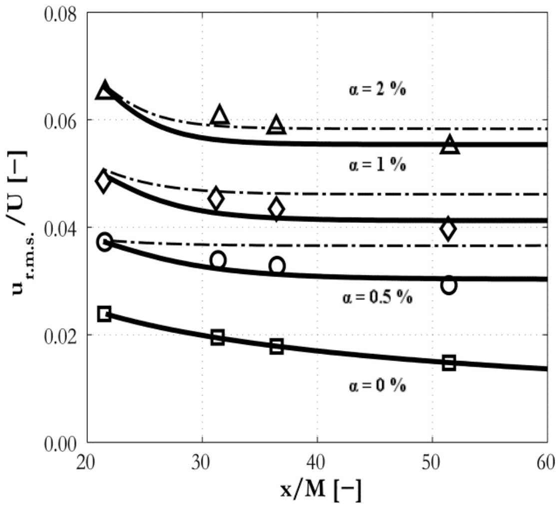


Figure 6. Axial development of turbulence in a bubbly flow. Model results with CF model (— reduced $K_{BI}$; –·– $K_{BI} = 0.25$) are compared against the data from Lance and Bataille (1991) at different void fractions.

### 4.3 Reynolds stress model

The bubble-induced turbulence model CF, optimized in the previous section, was then included in a Reynolds stress multiphase formulation, the validation of which against the same experimental database is the main subject of this section. A first comparison is shown in Figure 7 for experiments LB1, W3 and H1. These three experiments were selected as being the only cases in the database for which the r.m.s. of wall-normal velocity fluctuations were available. In particular, the models of Gibson and Launder (1978), Naot and Rodi (1982) and Speziale et al. (1991) are compared (which will be referred to in the following as GL, NR and SSG, respectively).

Experiment LB1 (Figure 7 a-d) is used here to summarize findings which were already discussed by Colombo et al. (2015). In particular, the authors noted that a linearly decreasing wall reflection term in the pressure-strain correlation, if still felt near the centre of the pipe, could interact with the flat turbulence profile generated by the presence of the bubbles, giving rise to an increase in the wall-normal velocity fluctuations towards the pipe axis. From radial momentum balances at steady-state, a gradient in the water wall-normal (specified $y$ below) r.m.s. introduces a radial pressure gradient with a lower pressure near the pipe axis, which remains unbalanced in the air momentum equation due to the low density of the air:

$$-(1-\alpha)\frac{\partial}{\partial y}\left[p+\rho_w\overline{v_w v_w}\right]+F_{l,w}+F_{w,w}+F_{td,w}=0 \tag{35}$$

$$-\alpha\frac{\partial}{\partial y}\left[p+\rho_a\overline{v_a v_a}\right]+F_{l,a}+F_{w,a}+F_{td,a}=0 \tag{36}$$

This pressure gradient pushes the bubbles towards the axis, until it is balanced by the lift force generated by the water velocity gradient sustained by the higher void fraction in the centre. This effect can be seen in Figure 7 a-d for the GL model, which includes a linear damping function of the wall reflection term in the pressure-strain correlation. The same effect is not appearent for the NR model, whose quadratic damping (Eq. (28) and Eq. (29)) assures a faster decay of the wall reflection effects with distance from the wall. This is illustrated in Figure 8a, where the wall reflection damping for both the GL and NR models is depicted. Clearly, wall effects decay more rapidly for NR and become negligible from $r/R \sim 0.5$. In contrast, they are still felt in the pipe centre for GL. Even if this does not trigger any unphysical behaviour in a single-phase flow, the same is not true in two-phase flows. As shown in Figure 8b, therefore, the presence of the bubbles generates a flatter turbulence profile. In the figure, the streamwise velocity fluctuations are similar for experiment H1, where the void fraction is low. For W3, however, which has a higher void fraction, the streamwise velocity fluctuations are almost flat from $r/R \sim 0.8$ to the pipe centre for the two-phase flow, whereas they are still decreasing until $r/R \sim 0.3$ in single-phase flow.

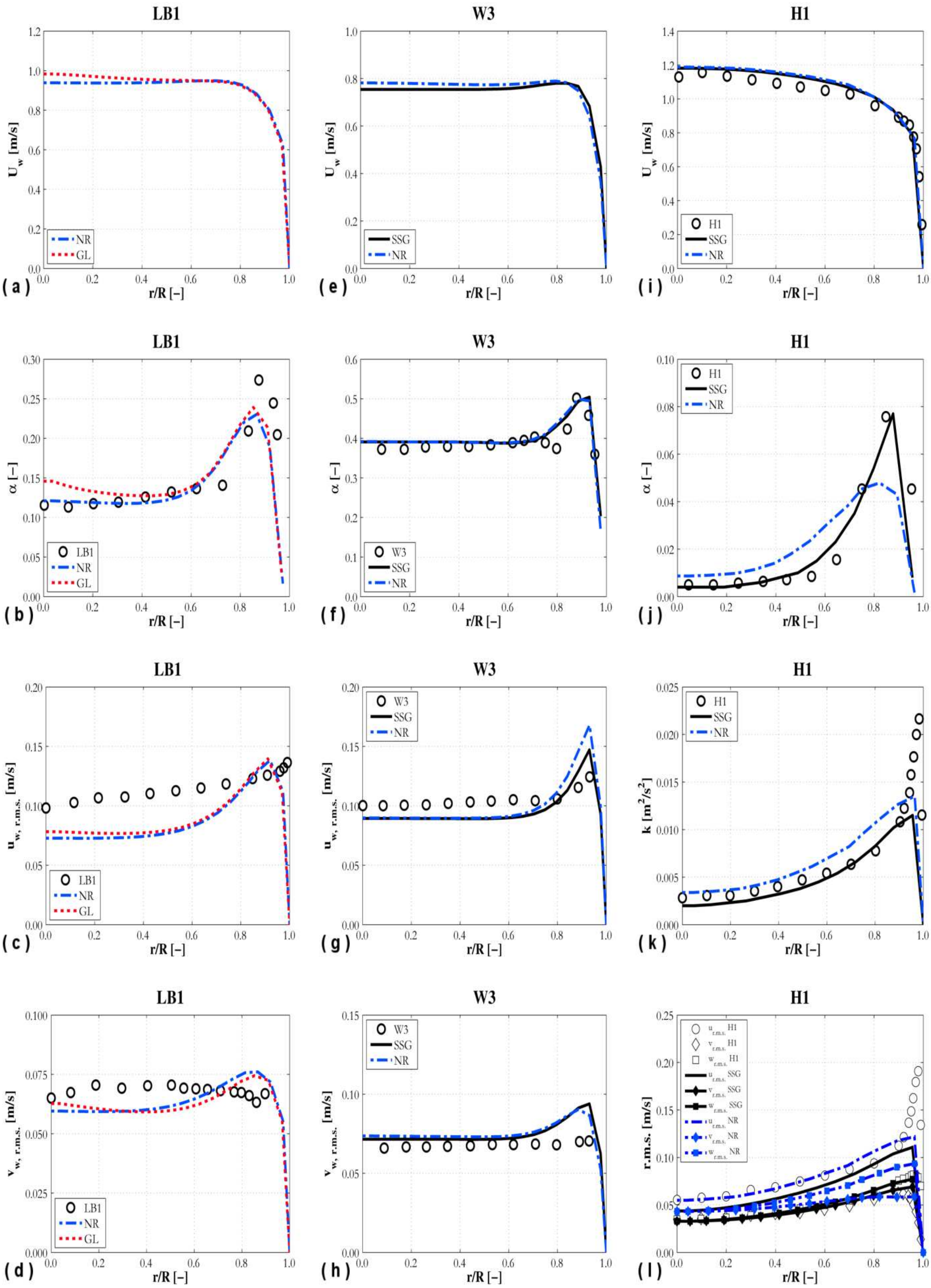


Figure 7. Radial profiles of predicted water velocity, void fraction, streamwise and wall-normal velocity fluctuations from different RSM compared against experiments LB1, W3 and H1 (from left to right). SSG: Speziale et al. (1991); NR: Naot and Rodi (1982); GL: Gibson and Launder (1978).

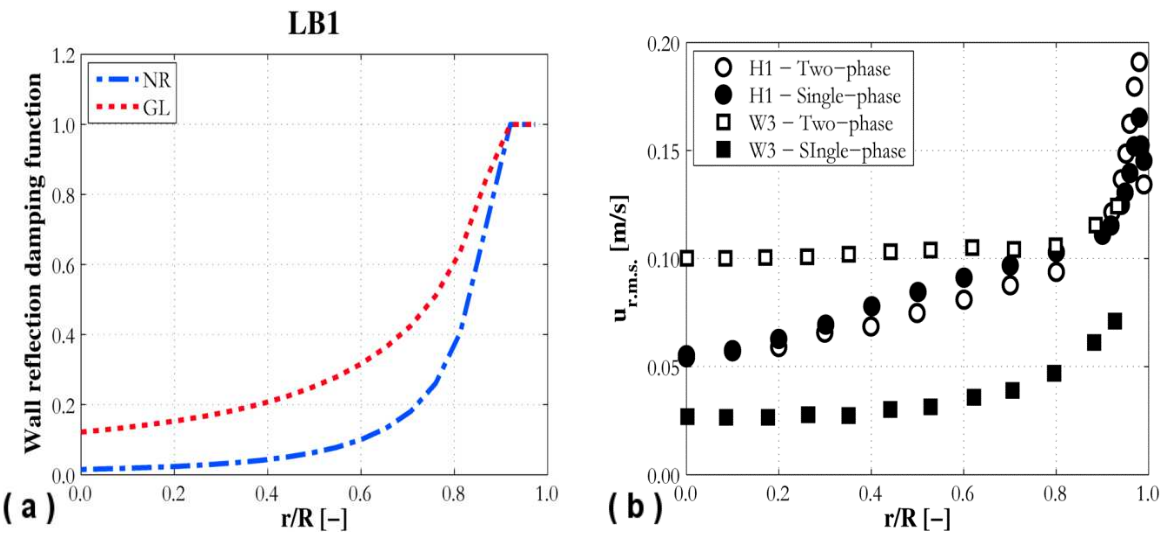


Figure 8. (a) Comparison between wall reflection damping as a function of the radial coordinate. NR: Naot and Rodi (1982); GL: Gibson and Launder (1978). (b) Experimental radial profiles of r.m.s. of streamwise velocity fluctuations in single- and two-phase flow for experiments H1 and W3.

Interaction of the wall effects in Figure 8a with the flat turbulence profile in Figure 8b generates the increase in the wall-normal velocity fluctuations (Figure 7d) and the unphysical void fraction increase in the pipe centre (Figure 7b). In constrast, the radial stress remains flat towards the pipe centre for NR and predictions are in agreement with experiments. In Colombo et al. (2015), the NR model was selected for additional simulations. Here, instead, the NR model is compared with the more advanced SSG formulation for experiments W3 and H1. Results are summarized in Figure 7 e-l. For experiment W3, the two models are in agreement with experimental data and with each other's predictions as well. The main difference is a more enhanced peak in the water velocity profile (the so-called "chimney effect") near the wall for the SSG, an effect that was already noted to characterize RSM simulations (Colombo et al., 2015). The SSG does not account explicitly for any wall reflection effects, these being unnecessary (Speziale, 1996), and it does not show unphysical behaviour in the void distribution at the pipe centre.

For the H1 experiment (Figure 7 i-l), which is the case with the lowest void fraction in the entire database, some differences are found between the two models. Similar mean velocity profiles are shown (Figure 7i), which are in good agreement with experiments. The SSG model is more accurate in the prediction of the near-wall peak in the void fraction, which is instead underestimated by NR (Figure 7j). SSG also predicts a lower turbulence kinetic energy (Figure 7k), which is more in agreement with experiments near the wall, but it is for the single Reynolds normal stresses that the major differences are found (Figure 7l). NR is more accurate in predicting the streamwise velocity fluctuations, which are underestimated by the SSG. The latter, instead, better predicts the wall-normal and azimuthal velocity fluctuations. In particular, both these stresses are well predicted for the whole radial profile and, in agreement with experiment, they differ amongst each other only in the region very close to the wall and, even in this region, the difference is limited. In contrast, both the wall-normal and the azimuthal velocity fluctuations are overestimated by the NR model, which also overestimates their difference in the near-wall region. Since the difference between $v_{r.m.s.}$ and $w_{r.m.s.}$ for the NR model is entirely due to wall reflection effects, the pressure-strain model, even if improved with respect to GL, still does not achieve a satisfactory accuracy. In particular, wall reflection effects are still felt for half the pipe radius, although the experimental evidence suggests they should be limited to a thinner region close to the wall.

In view of these results, the SSG model was chosen for the remaining simulations. It is a more advanced model, quadratically non-linear in the anisotropy tensor, and has proven superior to the linear formulation of Launder et al. (1975) in a variety of flow conditions (Speziale et al., 1991). As noted, the formulation applied here does not include any wall refelction effects, even if they did have a decisive influence on the accuracy of both the linear models, GL and NR. Efforts have been made in the past to include wall reflection effects in near-wall closures for the SSG model, which have not been considered here (So et al., 1994). However, as pointed out by Speziale (1996), the SSG yields acceptable results even in wall-bounded turbulent flows, and the need for the incorporation of wall reflection effects is more related to deficiencies in linear pressure-strain models.

Additional comparisons were made between the SSG Reynolds stress formulation and the $k$-$\varepsilon$ model. Radial profiles of liquid velocity, void fraction and liquid streamwise velocity fluctuations are shown in Figure 9 for experiments W2, LB2 and S2. Satisfactory agreement is achieved by both models. As already observed, with respect to the flat profile of the $k$-$\varepsilon$ model, the RSM shows a slight peak near the wall in the liquid velocity profile, followed by a dip towards the centre of the pipe. Even if it does not compromise the overall accuracy of the model, this might be attributable to the sensitivity of the RSM to the drag caused by bubbles moving at a higher velocity and with a higher concentration near the wall, and its effect on the liquid phase. In addition, this effect may not be completely unrealistic since, even if with a lower magnitude, a slightly higher velocity near the wall characterizes experiments W1 (Figure 4a) and W2 (Figure 9a). In the calculated profiles, this behaviour is more relevant for the LB2 experiment (Figure 9d), causing a slight underestimation of the liquid velocity in the centre of the pipe. For the $k$-$\varepsilon$ model, the same effect is shown only in experiment S2 (Figure 9g). Additional discussion on this subject is provided in the following section, where the impact of different drag models on the liquid velocity profile is discussed. Considering the void fraction and streamwise velocity fluctuations, the RSM shows a slightly lower near-wall peak of the void fraction and a lower turbulence level in the pipe centre. The latter is instead higher in the near-wall region, as a consequence of the differences in the velocity profile previously discussed. In general, results from the two models are very similar and in satisfactory agreement with experiments. Indeed, the $k$-$\varepsilon$ model has been proved to be sufficiently accurate when predicting velocity and void fraction profiles inside vertical pipes. In the context of the present work, pipe flows allowed validation of the multiphase Reynolds stress formulation and benchmarking against the *k*-ε model. Once validated, the improved ability of a Reynolds stress formulation to represent the turbulence field can be exploited for the prediction of more complex conditions, or flows that are affected by known shortcomings of two-equation turbulence models.

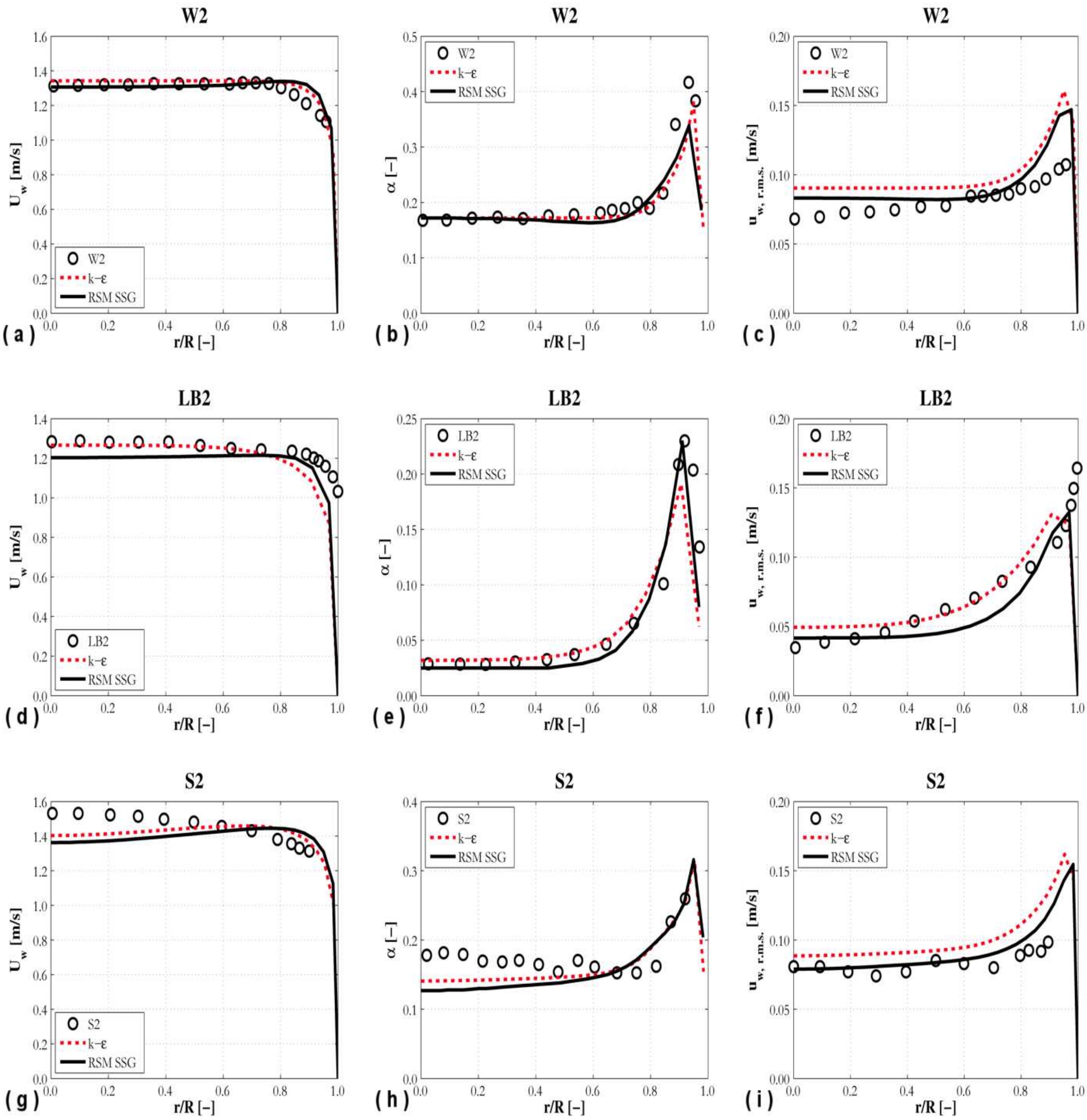


Figure 9. Radial profiles of predicted water velocity, void fraction and streamwise r.m.s. of velocity fluctuations for the *k*-ε and the Reynolds stress SSG model (RSM SSG) compared against experiments W2, LB2 and S2 (from top to bottom).

### 4.4 Drag model

In this section, both the $k$-$\varepsilon$ model and the RSM optimized in the previous section of the paper are used to evaluate the accuracy of different drag models. In Figure 10, liquid and air velocities, void fraction, liquid streamwise velocity fluctuations (or turbulence kinetic energy) and relative velocity radial profiles calculated with the $k$-$\varepsilon$ model are compared against experiments S2 and H1. Results from the drag model of Wang (1994), Tomiyama et al. (1998) and Tomiyama et al. (2002a) combined with the Welleck et al. (1966) correlation for the bubble aspect ratio are included. Experiment S2 is particularly relevant, since it is the only case were a distinct dip in the liquid velocity was found using the $k$-$\varepsilon$ model towards the centre of the pipe. In Figure 10 a-d, no significant differences are found beween Wang (1994) and Tomiyama et al. (1998), for which radial proflies are similar for all the physical quantities considered. In addition, the introduction of the void fraction correction in Eq. (11) produced negligible differences. Instead, significant differences are visible with the correlation of Tomiyama et al. (2002a), used together with the Welleck et al. (1966) correlation for the bubble aspect ratio. In addition to the higher drag coefficient that causes a lower relative velocity in the pipe centre, the drag coefficient further increases near the wall, generating a reduction in the relative velocity. Even if good quantitative agreement is not obtained, the relative velocity reduction in the near-wall region is in qualitative agreement with the experiment (Figure 10d). In the centre of the pipe, however, the accuracy of the prediction worsens. Changes in the relative velocity are also reflected in the void fraction and velocity profiles (Figure 10 a-b). For the velocity in particular, no dip towards the pipe centre is observed and the predictions are significantly improved, in particular for the liquid (Figure 10a). Similar results are found for  experiment H1 (Figure 10 e-h). In this case, quantitatively good agreement is also obtained with Tomiyama et al. (2002a) for the relative velocity near the wall (Figure 10h). Unfortunately, no measurements of the relative velocity are available near the pipe centre. With respect to the S2 experiments, no significant differences occur with the change of the drag model in the liquid velocity and the void fraction, which remain close to those obtained with the Wang (1994) drag model, and in agreement with experiments (Figure 10 e-f). In regards to experiment H1, the drag correction due to Legendre and Magnaudet (1998) was also tested. As shown in Figure 10h, this model did not give satisfactory agreement with data and its predictions were generally characterized by an excessive correction, which implies a limit to its effect is necessary. In view of these results, it was not adopted in successive simulations.

Comparisons were repeated for the Wang (1994) and Tomiyama et al. (2002a) approaches with the RSM (Figure 11). Similarly to the previous comparisons, the drag correlation of Tomiyama et al. (2002a) improves the relative velocity predictions near the wall for S2 (Figure 11d). This allows more accurate estimations of the water and air velocity profiles (Figure 11a). Even if the dip towards the pipe centre is still present, its magnitude is reduced with respect to the Wang (1994) model predictions. However, the accuracy in the pipe centre is low. Differences in the void fraction and the velocity fluctuations are lower, and both models are in reasonable agreement with the experiments (Figure 11 b-c). Considering experiment H1, similar predictions are obtained for the liquid velocity, the void fraction and the r.m.s. of velocity fluctuations (Figure 11 e-g). In agreement with the $k$-$\varepsilon$ comparisons in Figure 10, the relative velocity is also improved near the wall, where the Tomiyama et al. (2002a) predictions are in agreement with the data (Figure 11h).

In summary, and despite the deteriorating accuracy of predictions in the pipe centre, the improvements obtained in the near-wall region encourage use of the Tomiyama et al. (2002a) correlation to account for bubble aspect ratio in the drag model. Further validation with additional experimental data is required, in particular to confirm the lower accuracy in the pipe core region. If the latter is confirmed, additional work would be desirable to further improve the drag model, maintaining the same accuracy in the near-wall region without deteriorating it in the pipe centre. Finally, it must be pointed out that changes in the drag coefficent near the wall had a large impact on the magnitude of the lift and wall forces, being both functions of the relative velocity. Lift and wall forces essentially determine the void fraction radial profile in these kinds of flow, therefore, to maintain the same accuracy in the void fraction radial distribution, it was necessarry to re-optimize the wall force coefficients to $C_{w1}$ = -0.4 and $C_{w2}$ = 0.3 for the *k*-*ε* model, and $C_{w1}$ = -0.65 and $C_{w2}$ = 0.45 for the RSM. The differences between these two sets of values can be attributed to the differing interactions between the velocity, lift and wall forces and the turbulence field. A summary of the combination of models and model coefficients, together with the data used for validation, can be found in Table 3.

Table 3. Models and model coefficients tested and data used for validation.

| **Turbulence** | **Drag** | **Lift** | **Wall** | **Data** |
|---|---|---|---|---|
| *k*-*ε*, RSM | Wang (1994) | $C_L = 0.1$ WP<br>$C_L = -0.05$ CP | $C_{w,1} = -0.055$<br>$C_{w,2} = 0.09$ | Whole Database |
| *k*-*ε* | Tomiyama et al. (2002a) | $C_L = 0.1$ WP<br>$C_L = -0.05$ CP | $C_{w,1} = -0.4$<br>$C_{w,2} = 0.3$ | H1, S2, W4,<br>K1, K2, K3, K4 |
| RSM | Tomiyama et al. (2002a) | $C_L = 0.1$ WP<br>$C_L = -0.05$ CP | $C_{w,1} = -0.65$<br>$C_{w,2} = 0.45$ | H1, S2, W4,<br>K1, K2, K3, K4 |

WP wall-peaked void profiles
CP core-peaked void profiles

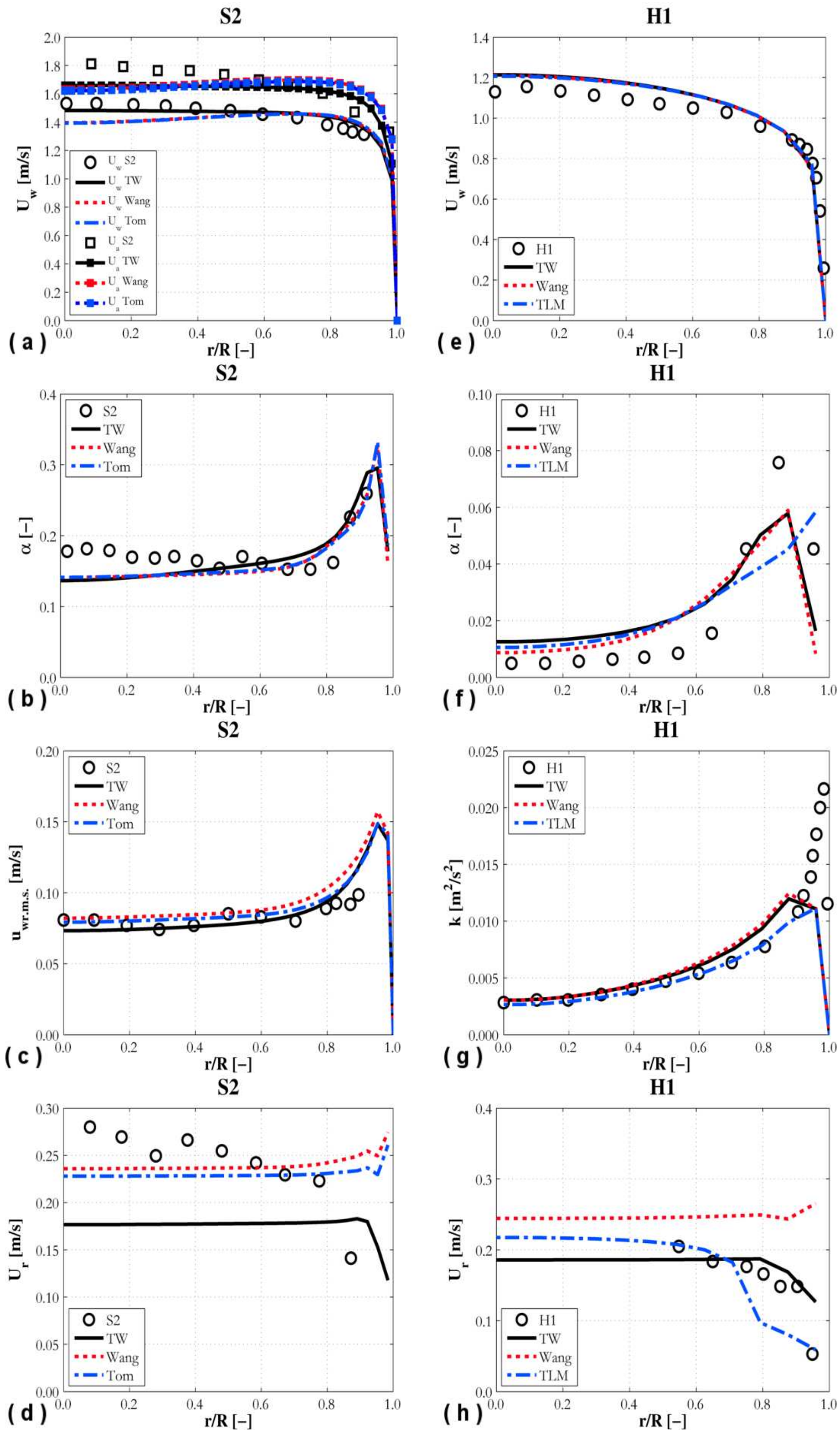


Figure 10. Radial profiles of predicted water (and air for S2) velocity, void fraction, streamwise r.m.s. of velocity fluctuations (turbulence kinetic energy for H1) and relative velocity from *k*-ε and different drag models compared against experiments S2 and H1 (from left to right). TW: Tomiyama et al. (2002a) + Welleck et al. (1966); Wang: Wang (1994); Tom: Tomiyama et al. (1998); TLM: Tomiyama et al. (1998) + Legendre and Magnaudet (1998)

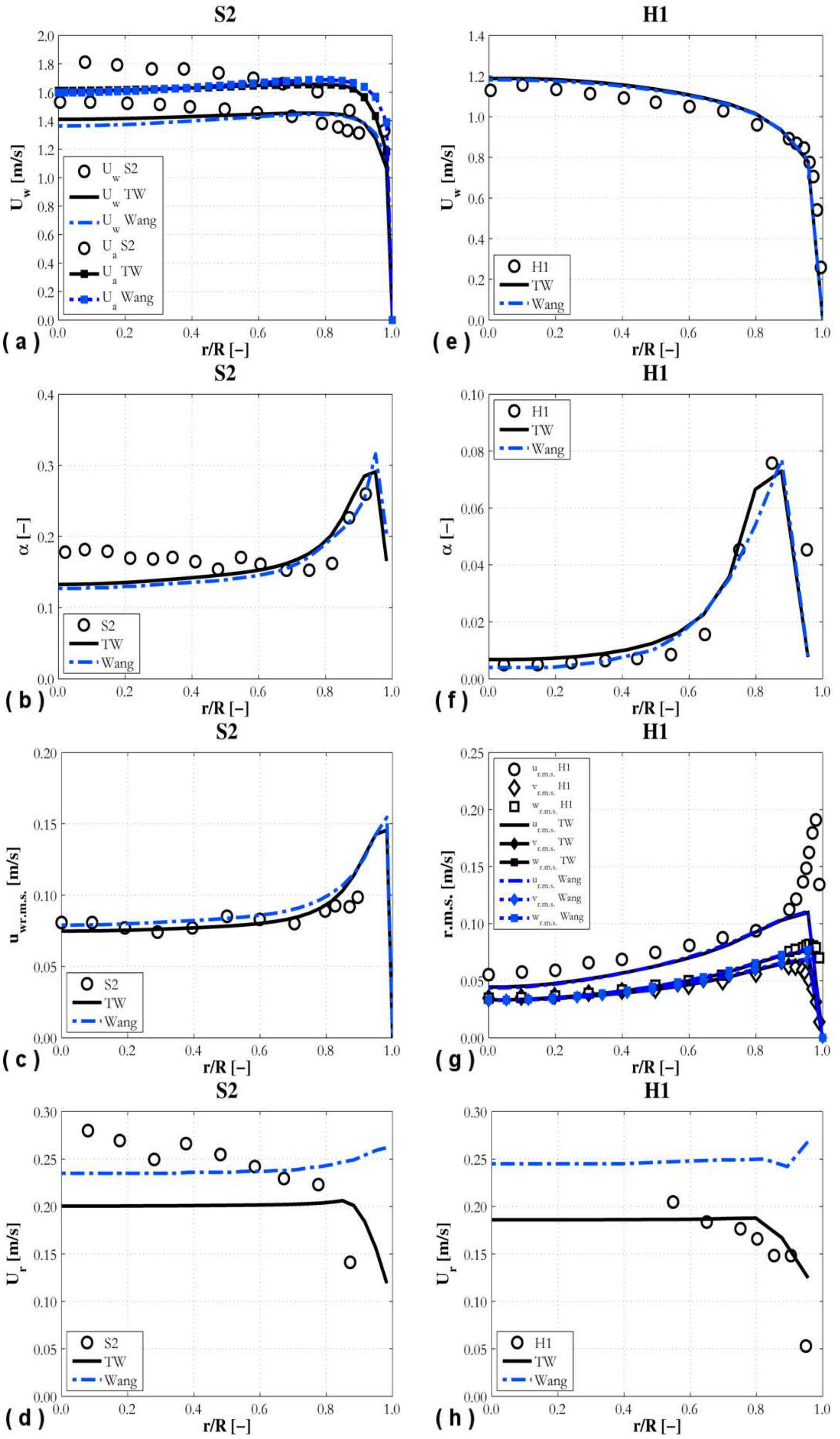


Figure 11 Radial profiles of predicted water (and air for S2) velocity, void fraction, streamwise r.m.s. of velocity fluctuations and relative velocity from RSM and different drag models compared against experiments S2 and H1 (from left to right). TW: Tomiyama et al. (2002a) + Welleck et al. (1966); Wang: Wang (1994).

### 4.5 Downward flows

Finally, for additional validation, comparison was made against some downward pipe flows from the experimental measurements of Wang et al. (1987) and Kashinsky and Randin (1999). Figure 12 shows experiments W4, K1 and K4 and, in particular, radial profiles of water velocity, void fraction and streamwise velocity fluctuations. For Kashinsky and Randin (1999), water velocity and streamwise r.m.s. fluctuating velocities are normalized by the pipe centre velocity, in line with the authors' original database. Figure 12 highlights the general characteristics of a bubbly downward flow. The lift force and wall force are both directed towards the pipe centre and, therefore, no void peak is present in the near-wall region. A bubble-free layer occupies the immediate vicinity of the wall, followed by an almost flat distribution towards the pipe centre. Downward flows are also characterized by an almost flat velocity profile and, in addition, a water velocity peak, generally known as the "chimney effect" (Wang et al., 1987), is observed near the wall in some of the experiments (Figure 12a and Figure 12d). The latter is due to the water velocity being higher than the air velocity, so that bubbles act to retard the flow in these cases. Therefore, higher liquid velocities can be found in the low void fraction region near the wall.

Calculated water velocity and void fraction profiles are in general in good agreement with data for both models, even if some discrepancies with the experiments can still be observed. The wall peak in some of the water velocity profiles seems difficult to predict, in particular for experiment K1, where it is underestimated by both the $k$-ε model and the RSM (Figure 12d). The agreement is better for K4, which does not show the water velocity peak near the wall (Figure 12g). The void fraction, despite generally good agreement, is overestimated for K1 (Figure 12e). Given the overall accuracy found throughout the entire work reported, this may be attributed to discrepancies between experimental and simulated conditions.

No significant differences are found between the $k$-ε model and the RSM in the calculated water streamwise r.m.s. of velocity fluctuations (Figure 12c, Figure 12f and Figure 12i). The $k$-ε model tends to predict a slightly higher level of turbulence, provided that the drag model, which governs the amount of the bubble-induced contribution, remains the same. For the $k$-$\varepsilon$ model, simulations were made with the Wang (1994) drag model for experiments W4 and K1 and with Tomiyama et al. (2002a) combined with Welleck et al. (1966) for experiment K4. For W4 (Figure 12c) and K1 (Figure 12f), the $k$-$\varepsilon$ model predicts the highest velocity fluctuations, whereas for K4 (Figure 12i) they are lower with respect to the RSM with Wang (1994) drag, but higher with respect to RSM with Tomiyama et al. (2002a). Velocity fluctuations are in agreement with measurements for experiments W4 and K4, but they are underestimated for the K1 experiment. Given the differences in the predicted velocity fluctuations, two additional issues are deserving of further consideration. Downward flows were exploited to further test the drag models, and the results appear in line with the conclusions derived in the previous section. The drag model of Tomiayama et al. (2002a) might again underestimate the relative velocity in the centre of the pipe, even if only indirect indications are available for these experiments. In particular, the lower void fraction calculated with Tomiyama et al. (2002a) indicates that the air flows at a higher velocity, and is therefore closer to the water velocity (Figure 12b, Figure 12e and Figure 12h). In addition, the lower velocity fluctuations obtained with Tomiyama et al. (2002a) suggest a lower bubble-induced turbulence contribution, which is a function of the relative velocity (Figure 12c, Figure 12f and Figure 12i). On the other hand, improvements in the velocity and void fraction profiles are observed, in particular for experiment K4. In more detail, the RSM results obtained with the Wang (1994) drag model show velocity and void fraction peaks near the wall that are not confirmed by the experimental data (Figure 12 g-h). Results for the different drag models are more similar for experiment K1 (Figure 12 d-f), which is characterized by the lowest bubble diameter (0.8 mm). At low bubble diameter, the relative velocity between the phases is lower since bubbles tend to follow the water flow more closely. Therefore, differences between the models are negligible under these conditions. In addition, the shape of the bubbles is closer to spherical, therefore the effect of the aspect ratio correction of Welleck et al. (1966) also becomes negligible.

Focusing on the bubble-induced turbulence model, it should be noted that turbulence predictions are in agreement with experiments for W4 ($d_B$ ~ 3 mm) and K4 ($d_B$ = 1.5 mm), whereas they are underestimated for K1 ($d_B$ = 0.8 mm). This suggests some difficulties in handling low bubble diameter conditions, where the lengthscale of the bubbles is less comparable with the lengthscale of the turbulence. In these conditions, conversion of drag work to turbulence kinetic energy in the bubble wakes may not be the dominant bubble-induced turbulence contribution, due to both the smaller lengthscale of the bubble and the lower relative velocity. In this regard, future efforts should be directed towards the development of a more advanced model, able to account for "pseudo-turbulence" due to liquid displacement by random bubble movements (Lance and Bataille, 1991). For the mentioned conditions, the smaller diameter of the bubbles should allow for a higher contribution due to the increased ability of turbulence to displace bubbles after their interaction with turbulent eddies.

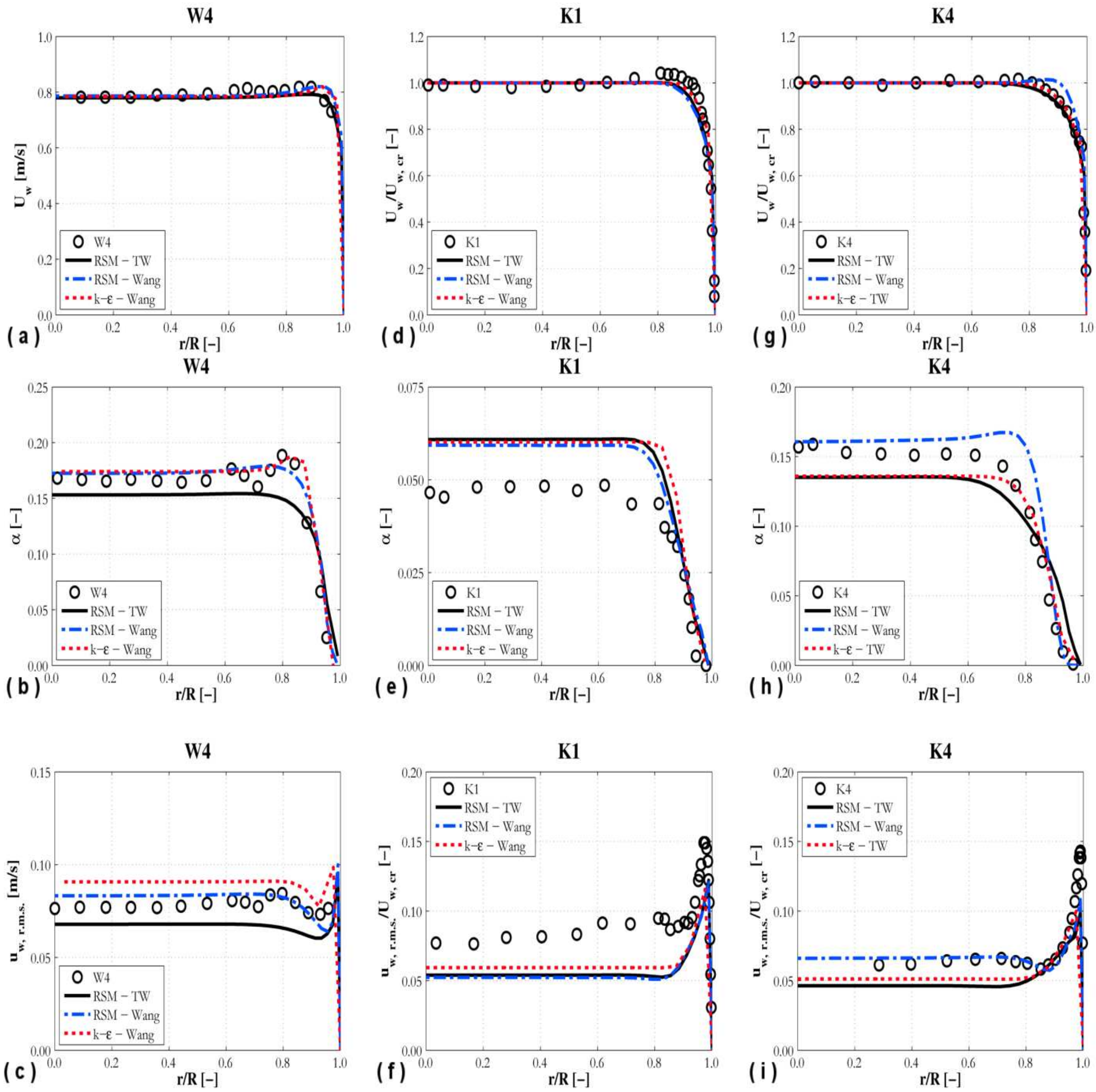


Figure 12 Radial profiles of predicted water velocity, void fraction and streamwise r.m.s. of velocity fluctuations from *k*-ε and SSG RSM and different drag models compared against experiments W4, K1, and K4 (from left to right). TW: Tomiyama et al. (2002a) + Welleck et al. (1966); Wang: Wang (1994).

# 5. Conclusions

Adiabatic air-water upward and downward bubbly flows in pipes were studied in this work using a two-fluid Eulerian-Eulerian CFD model and the STARCCM+ code. An experimental database including 19 flow conditions was assembled using measurements from 6 different literature sources. The large number of experiments was aimed at extending the model validation over a wide range of conditions. The main subject of the paper has been the simulation of multiphase turbulence in bubbly flows due to its significance in many related areas, such as bubble coalescence/break-up in population balance approaches and wall boiling models. With the aim of improving the ability of available CFD approaches to predict the characteristics of bubbly flows, pipe flows were selected as the test case. Pipe flows provide relatively simple flow conditions with respect to other complex flows encountered in practice, and have also received a great deal of attention in previous studies.

Overall, good agreement with experimental data was obtained for liquid velocity and void fraction distributions over the whole database, which includes upward and downward flows and wall-peaked and core-peaked void fraction profiles. In view of its importance for the correct prediction of turbulence in these flows, an improved bubble-induced turbulence model has been developed, starting from an existing formulation. The model includes source terms for the turbulence kinetic energy and the turbulence energy dissipation rate, under the hypothesis that the bubble contribution is entirely due to conversion of the work of the drag force to turbulence kinetic energy inside the bubble wakes. In the turbulence energy dissipation rate source, a mixed timescale is used, calculated from the water turbulence velocity scale and the bubble length scale. After comparison with experiments, the modulation of the turbulence kinetic energy source was found to guarantee satisfactory accuracy in the prediction of the velocity fluctuations over the whole database, and an improved accuracy with respect to other available models. Accounting for more physical influences on the modulating function, limited to a constant value in the present work, will be pursued in future, provided that a larger number of detailed experimental measurements are available. The ability of the model to predict the axial development of turbulence was also validated against data for uniform, grid-generated, turbulent bubbly flows. Some drawbacks of the model were identified at low bubble diameter, where calculations exhibited an underestimation of the velocity fluctuations. This result suggests the need for a more complex bubble-induced turbulence formulation to improve the predictive accuracy for such bubbles. More specifically, it seems necessary to also account for the generation of turbulence through liquid displacement by bubble random motion, which may be more important than generation in the bubble wakes when the bubble length scale is significantly lower than the turbulence length scale and the bubbles more closely follow the liquid flow.

A multiphase Reynolds stress formulation based on the SSG model, combined with the improved bubble-induced turbulence model, was able to predict with satisfactory accuracy velocity and void fraction distributions in these flows, and the anisotropy of the Reynolds stresses. Possible issues were identified in the formulation of wall reflection terms, which are frequently added to linear pressure-strain models to account for the effect of the presence of a solid wall. If not properly limited to the near-wall region, they can interact with the two-phase field, generating unphysical behaviour in the phase distribution at the centre of the pipe. In this regard, the more advanced quadratic SSG closure was identified as the best option in the present work. For the pipe flows considered, good predictions of the bubbly flows were also obtained with the $k$-$\varepsilon$ turbulence model. However, the superior ability of a validated Reynolds stress formulation to describe the turbulence field and its anisotropy would benefit the simulation of more complex flows, particularly given the known shortcomings of two-equation turbulence models.

Lastly, different drag models were also evaluated. Introducing the effect of bubble aspect ratio in the drag correlation, as in the model of Tomiyama et al. (2002a), allowed the more accurate calculation of velocity profiles near the wall. In this work, the aspect ratio was evaluated through the correlation of Welleck et al. (1966). In contrast, it would appear that relative velocity results are underestimated in the centre of the pipe, such that further testing is required. If the latter is confirmed, further research will be necessary to maintain the advantages of including the effect of bubble aspect ratio in the near-wall region without loosing at the same time model accuracy in the pipe centre.

## Acknowledgements

The authors gratefully acknowledge the financial support of the EPSRC under grant EP/K007777/1, Thermal Hydraulics for Boiling and Passive Systems, part of the UK-India Civil Nuclear Collaboration.

The authors are also grateful to Dr. Andrew Splawski and Dr. Simon Lo from CD-adapco for the valuable technical and scientific support.

## References

Antal, S.P., Lahey Jr, R.T., Flaherty, J.E., 1991. Analysis of phase distribution in fully developed laminar bubbly two-phase flow. Int. J. Multiphas. Flow 17, 635-652.

Auton, T.R., 1987. The lift force on a spherical body in a rotational flow. J. Fluid Mech. 183, 199-218.

Behzadi, A., Issa, R.I., Rusche, H., 2004. Modelling of dispersed bubble and droplet flow at high phase fractions. Chem. Eng. Sci. 59, 759-770.

Besnard, D.C. and Harlow, F.H., 1989. Turbulence in multiphase flow. Int. J. Multiphas. Flow 14, 679-699.

Bunner, B. and Tryggvason, G., 2002a. Dynamics of homogeneous bubbly flows. Part 1. Rise velocity and miscrostructure of the bubbles. J. Fluid Mech. 466, 17-52.

Bunner, B. and Tryggvason, G., 2002b. Dynamics of homogeneous bubbly flows. Part 2. Velocity fluctuations. J. Fluid Mech. 466, 53-84.

Burns, A.D., Frank, T., Hamill, I., Shi, J.M., 2004. The Favre averaged drag model for turbulent dispersion in Eulerian multi-phase flows. 5th International Conference on Multiphase Flow, Yokohama, Japan, May 30 – June 4.

CD-adapco, 2014. STAR-CCM+® Version 9.06 User Guide.

Celata, G.P., D'Annibale, F., Di Marco, P., Memoli, G., Tomiyama, A., 2007. Measurements of rising velocity of a small bubble in a stagnant fluid in one- and two-component systems. Exp. Therm. Fluid Sci. 31, 609-623.

Colombo, M., Fairweather, M., Lo, S., Splawski, A., 2015. Multiphase RANS simulation of turbulent bubbly flows. 16th International Topical Meeting on Nuclear Reactor Thermal Hydraulics, Chicago, USA, August 30 – September 4 (accepted for presentation).

Crowe, C.T., 2000. On models for turbulence modulation in fluid-particle flows. Int. J. Multiphas. Flow 26, 719-727.

Daly, B.J. and Harlow, F.H., 1970. Transport equations of turbulence. Phys. Fluids 13, 2634-2649.

Drew, D.A., 1983. Mathematical modeling of two-phase flow. Annu. Rev. Fluid Mech. 15, 261-291.

Drew, D.A. and Lahey Jr, R.T., 1981. Phase distribution mechanisms in turbulent two-phase flow in channels of arbitrary cross section. J. Fluids Eng. 103, 583-589.

Elghobashi, S.E. and Abou-Arab, T.W., 1983. A two-equation turbulence moodel for two-phase flows. Phys. Fluids 26, 931-938.

Ervin, E.A. and Tryggvason, G., 1997. The rise of bubbles in a vertical shear flow. J. Fluids Eng. 119, 443-449.

Gibson, M.M. and Launder, B.E., 1978. Ground effects on pressure fluctuations in the atmospheric boundary layer. J. Fluid Mech. 86, 491-511.

Gosman, A.D., Lekakou, C., Politis, S., Issa, R.I., Looney, M.K., 1992. Multidimensional modeling of turbulent two-phase flows in stirred vessels. AIChE J. 38, 1946-1956.

Hibiki, T. and Ishii, M., 1999. Experimental study on interfacial area transport in bubbly two-phase flows. Int. J. Heat Mass Tran. 42, 3019-3035.

Hibiki, T. and Ishii, M., 2007. Lift force in bubbly flow systems. Chem. Eng. Sci. 62, 6457-6474.

Hibiki, T., Ishii, M., Xiao, Z., 2001. Axial interfacial area transport of vertical bubbly flows. Int. J. Heat Mass Tran. 44, 1869-1888.

Hosokawa, S. and Tomiyama, A., 2009. Multi-fluid simulation of turbulent bubbly pipe flow. Chem. Eng. Sci. 64, 5308-5318.

Hosokawa, S. and Tomiyama, A., 2013. Bubble-induced pseudo turbulence in laminar pipe flows. Int. J. of Heat Fluid Fl. 40, 97-105.

Ishii, M. and Hibiki, T., 2006. Thermo-fluid dynamics of two-phase flow. Springer.

Ishii, M. and Zuber, N., 1979. Drag coefficient and relative velocity in bubbly, droplet or particulate flows. AIChE J. 25, 843-855.

Kashinsky, O.N. and Randin, V.V., 1999. Downward bubbly gas-liquid flow in a vertical pipe. Int. J. Multiphas. Flow 25, 109-138.

Kataoka, I. and Serizawa, A., 1989. Basic equations of turbulence in gas-liquid two-phase flow. Int. J. Multiphas. Flow 15, 843-855.

Krepper, E., Lucas, D., Frank, T., Prasser, H.M., Zwart, P.J., 2008. The inhomogeneous MUSIG model for the simulation of polydispersed flows. Nucl. Eng. Des. 238, 1690-1702.

Krepper, E., Rzehak, R., Lifante, C., Frank, T., 2013. CFD for subcooled flow boiling: Coupling wall boiling and population balance models. Nucl. Eng. Des. 255, 330-346.

Jones, W.P. and Launder, B.E., 1972. The prediction of laminarization with a two-equation model of turbulence. Int. J. Heat Mass Tran. 15, 301-314.

Lahey Jr, R.T. and Drew, D.A., 2001. The analysis of two-phase flow and heat transfer using a multidimensional, four field, two-fluid model. Nucl. Eng. Des. 204, 29-44.

Lahey Jr, R.T., Lopez de Bertodano, M., Jones Jr, O.C., 1993. Phase distribution in complex geometry conduits. Nucl. Eng. Des. 141, 177-201.

Lance, M. and Bataille, J., 1991. Turbulence in the liquid phase of a uniform bubbly air-water flow. J. Fluid Mech. 222, 95-118.

Launder, B.E., Reece, G.J., Rodi, W., 1975. Progress in the development of a Reynolds-stress turbulence closure. J. Fluid Mech. 68, 537-566.

Legendre, D. and Magnaudet, J., 1998. The lift force on a spherical bubble in a viscous linear shear flow. J. Fluid Mech. 368, 81-126.

Liao, Y., Rzehak, R., Lucas, D., Krepper, E., 2015. Baseline closure model for dispersed bubbly flow: Bubble coalescence and breakup. Chem. Eng. Sci. 122, 336-349.

Liao, Y. and Lucas, D., 2009. A literature review of theoretical models for drop and bubble breakup in turbulent dispersion. Chem. Eng. Sci. 64, 3389-3406.

Liao, Y. and Lucas, D., 2010. A literature review on mechanisms and models for the coalescence process of fluid particles. Chem. Eng. Sci. 65, 2851-2864.

Liu, T.J., 1997. Investigation of wall shear stress in vertical bubby flow under different bubble size conditions. Int. J. Multiphas. Flow 23, 1085-1109.

Liu, T.J., 1998. The role of bubble size on liquid phase on liquid phase turbulent structure in two-phase bubbly flows. Proceedings of the 3rd International Conference on Multiphase Flow, Lyon, France, June 8-12.

Liu, T.J. and Bankoff, S.G., 1993a. Structure of air-water bubbly flow in a vertical pipe-I. Liquid mean velocity and turbulence measurements. Int. J. Heat Mass Tran. 36, 1049-1060.

Liu, T.J. and Bankoff, S.G. 1993b. Structure of air-water bubbly flow in a vertical pipe-II. Void fraction, bubble velocity and bubble size distribution. Int. J. Heat Mass Tran. 36, 1061-1072.

Lopez de Bertodano, M., Lahey Jr, R.T., Jones, O.C., 1994a. Development of a k-ε model for bubbly two-phase flow. J. Fluids Eng. 116, 128-134.

Lopez de Bertodano, M., Lahey Jr, R.T., Jones, O.C., 1994b. Phase distribution in bubbly two-phase flow in vertical ducts. Int. J. Multiphas. Flow 20, 805-818.

Lopez de Bertodano, M, Lee, S.J., Lahey Jr, R.T., Drew, D.A., 1990. The prediction of two-phase turbulence and phase distribution phenomena using a Reynolds stress model. J. Fluid Eng. 112, 107-113.

Lu, J. and Tryggvason, G., 2014. Bubble coalescence in channel flows. 67th Annual Meeting of the APS Division of Fluid Dynamics, San Francisco, USA, November 23-35.

Lucas, D., Beyer, M., Szalinski, L., Schutz, P., 2010. A new databse on the evolution of air-water flows along a large vertical pipe. Int. J. Therm. Sci. 49, 664-674.

Lucas, D., Krepper, E., Prasser, H.M., 2005. Development of co-current air-water flow in a vertical pipe. Int. J. Multiphas. Flow 31, 1304-1328.

Lucas, D., Krepper, E., Prasser, H.M., 2007. Use of models for lift, wall and turbulent dispersion forces acting on bubbles for poly-disperse flows. Chem. Eng. Sci. 62, 4146-4157.

Lucas, D. and Tomiyama, A., 2011. On the role of the lateral lift force in poly-dispersed bubbly flows. Int. J. Multiphas. Flow 37, 1178-1190.

Michiyoshi, I. and Serizawa, A., 1984. Turbulence in two-phase bubbly flow. Proceedings of the Japan-US Seminar on Two-Phase Flow Dynamics, Lake Placid, USA, July 29-August 3.

Mimouni, S., Archambeau, F., Boucker, M., Lavieville, J., Morel, C., 2010. A second order turbulence model based on a Reynolds stress approach for two-phase boiling flows. Part 1: Application to the ASU-annular channel case. Nucl. Eng. Des. 240, 2233-2243.

Mimouni, S., Lavieville, J., Seiler, N., Ruyer, P., 2011. Combined evaluation of second order turbulence model and polydispersion model for two-phase boiling flow and application to fuel assembly analysis. Nucl. Eng. Des. 241, 4523-4536.

Moraga, F.J., Bonetto, R.T., Lahey, R.T., 1999. Lateral forces on spheres in turbulent uniform shear flow. Int. J. Multiphas. Flow 25, 1321-1372.

Morel, C., 1997. Turbulence modeling and first numerical simulations in turbulent two-phase flows. Report SMTH/LDMS/97-023, CEA/Grenoble, France.

Nakoryakov, V.E., Kashinsky, O.N., Randin, V.V., Timkin, L.S., 1996. Gas-liquid bubbly flow in vertical pipes. J. Fluids Eng. 118, 377-382.

Naot, D. and Rodi, W., 1982. Numerical simulation of secondary currents in channel flow. J. Hydr. Eng. Div. - ASCE 108, 948-968.

Nigmatulin, R.I., 1979. Spatial averaging in the mechanics of heterogeneous and dispersed systems. Int. J. Multiphas. Flow 5, 353-385.

Politano, M.S., Carrica, P.M., Converti, J., 2003. A model for turbulent polydisperse two-phase flow in vertical channels. Int. J. Multiphas. Flow 29, 1153-1182.

Prasser, H.M., Beyer, M., Carl, H., Gregor, S., Lucas, D., Pietruske, H., Schutze, P., Weiss, F.P., 2007. Evolution of the structure of a gas-liquid two-phase flow in a large vertical pipe. Nucl. Eng. Des. 237, 1848-1861.

Prosperetti, A. and Tryggvason, G., 2009. Computational methods for multiphase flow. Cambridge University Press.

Rzehak, R. and Krepper, E., 2013a. CFD modeling of bubble-induced turbulence. Int. J. Multiphas. Flow 55, 138-155.

Rzehak, R. and Krepper, E., 2013b. Closure models for turbulent bubbly flows: A CFD study. Nucl. Eng. Des. 265, 701-711.

Sato, Y., Sadatomi, M., Sekoguchi, K., 1981. Momentum and heat transfer in two-phase bubbly flow-I. Theory. Int. J. Multiphas. Flow 7, 167-177.

Serizawa, A., Kataoka, I., Michiyoshi, I., 1975a. Turbulence structure of air-water bubbly flow-I. Measuring techniques. Int. J. Multiphas. Flow 2, 221-233.

Serizawa, A., Kataoka, I., Michiyoshi, I., 1975b. Turbulence structure of air-water bubbly flow-II. Local properties. Int. J. Multiphas. Flow 2, 235-246.

Serizawa, A., Kataoka, I., Michiyoshi, I., 1975c. Turbulence structure of air-water bubbly flow-III. Transport properties. Int. J. Multiphas. Flow 2, 247-259.

Shawkat, M.E., Ching, C.Y., Shoukri, M., 2007. On the liquid turbulence energy spectra in two-phase bubbly flow in a large diameter pipe. Int. J. Multiphas. Flow 33, 300-316.

Shawkat, M.E., Ching, C.Y., Shoukri, M., 2008. Bubble and liquid turbulence characteristics of bubbly flow in a large diameter vertical pipe. Int. J. Multiphas. Flow 34, 767-785.

So, R.M.C., Aksoy, H., Sommer, T.P., Yuan, S.P., 1994. Development of a near-wall Reynolds-stress closure based on the SSG model for the pressure-strain. NASA Contractor Report 4618.

So, S., Morikita, H., Takagi, S., Matsumoto, Y., 2002. Laser Doppler velocimetry measurement of turbulent bubbly channel flow. Exp. Fluids 33, 135-142.

Speziale, C.G., 1996. Modeling of turbulence transport equations. In: Gatski, T.B., Hussaini, M.Y., Lumley, J.L., (Eds.). Simulation and modeling of turbulent flows, Chapter 5, 185-242. Oxford University Press, New York.

Speziale, C.G., Sarkar, S., Gatski, T.B., 1991. Modelling the pressure-strain correlation of turbulence: An invariant dynamical system approach. J. Fluid Mech. 227, 245-272.

Tomiyama, A., Kataoka, I., Zun, I., Sakaguchi, T., 1998. Drag coefficients of single bubbles under normal and micro gravity conditions. JSME Int. J. B - Fluid T., 41, 472-479.

Tomiyama, A., Celata, G.P., Hosokawa, S., Yoshida, S., 2002a. Terminal velocity of single bubbles in surface tension dominant regime. Int. J. Multiphas. Flow 28, 1497-1519.

Tomiyama, A., Tamai, H., Zun, I., Hosokawa, S., 2002b. Transverse migration of single bubbles in simple shear flows. Chem. Eng. Sci. 57, 1849-1858.

Toutant, A., Labourasse, E., Lebaigue, O., Simonin, O., 2008. DNS of the interaction between a deformable buoyant bubble and a spatially decaying turbulence: A priori tests for LES two-phase flow modelling. Comput. Fluids 37, 877-886.

Troshko, A.A. and Hassan, Y.A., 2001. A two-equation turbulence model of turbulent bubbly flows. Int. J. Multiphas. Flow 27, 1965-2000.

Tryggvason, G. and Buongiorno, J., 2010. The role of direct numerical simulations in validation and verification. Computational Fluid Dynamics (CFD) for Nuclear Reactor Safety Applications OECD-NEA Workshop, Bethesda, USA September 14-16.

Ullrich, M., Maduta, R., Jakirlic, S., 2014. Turbulent bubbly flow in a vertical pipe computed by an eddy-resolving Reynolds stress model. Proceedings of the 10th International ERCOFTAC Symposium on Engineering Turbulence Modelling and Measurements, Marbella, Spain, September 17-19.

Wang, D.M., 1994. Modelling of bubble flow in a sudden pipe expansion. Technical Report II-34, BRITE/EuRam Project BE-4098.

Wang, S.K., Lee, S.J., Jones Jr, O.C., Lahey Jr, R.T., 1987. 3-D turbulence structure and phase distribution measurements in bubbly two-phase flows. Int. J. Multiphas. Flow 13, 327-343.

Welleck, R.M., Agrawal, A.K., Skelland, A.H.P., 1966. Shape of liquid drops moving in liquid media. AIChE J. 12, 854-862.

Wu, X., Baltzer, J.R., Adrian, R.J., 2012. Direct numerical simulation of a 30R long turbulent pipe flow at $R^+ = 685$: large- and very-large scale motions. J. Fluid Mech. 698, 235-281.

Yadigaroglu, G., 2014. CMFD and the critical-heat-flux grand challenge in nuclear thermal-hydraulics – A letter to the editor of this special issue. Int. J. Multiphas. Flow 67, 3-12.

Yao, W. and Morel, C., 2004. Volumetric interfacial area prediction in upward bubbly two-phase flow. Int. J. Heat Mass Tran. 47, 307-328.

Yeoh, G.H. and Tu, J.Y., 2006. Two-fluid and population balance models for subcooled boiling flow. Appl. Math. Model. 30, 1370-1391.